YALE
PEABODY
MUSEUM

P.O. BOX 208118 | NEW HAVEN CT 06520-8118 USA | PEABODY.YALE. EDU

JOURNAL OF MARINE RESEARCH

The *Journal of Marine Research,* one of the oldest journals in American marine science, published important peer-reviewed original research on a broad array of topics in physical, biological, and chemical oceanography vital to the academic oceanographic community in the long and rich tradition of the Sears Foundation for Marine Research at Yale University.

An archive of all issues from 1937 to 2021 (Volume 1–79) are available through EliScholar, a digital platform for scholarly publishing provided by Yale University Library at https://elischolar.library.yale.edu/.

Requests for permission to clear rights for use of this content should be directed to the authors, their estates, or other representatives. The *Journal of Marine Research* has no contact information beyond the affiliations listed in the published articles. We ask that you provide attribution to the *Journal of Marine Research*.

Yale University provides access to these materials for educational and research purposes only. Copyright or other proprietary rights to content contained in this document may be held by individuals or entities other than, or in addition to, Yale University. You are solely responsible for determining the ownership of the copyright, and for obtaining permission for your intended use. Yale University makes no warranty that your distribution, reproduction, or other use of these materials will not infringe the rights of third parties.

This work is licensed under a Creative Commons Attribution-NonCommercial-ShareAlike 4.0 International License.
https://creativecommons.org/licenses/by-nc-sa/4.0/

Journal of Marine Research, 49, 109–151, 1991

Micropatchiness, turbulence and recruitment in plankton

by Cabell S. Davis,[1] Glenn R. Flierl,[2] P. H. Wiebe[1]
and P. J. S. Franks[1]

ABSTRACT

A series of models are presented which examine the relative importance of microscale patchiness and turbulence to growth and recruitment in planktonic consumers. The analyses apply over scales from centimeters to meters (e.g. from copepods to fish larvae), and we assume food-limited conditions, since, otherwise, patchiness would not affect growth. A model of individual growth response to fluctuating food is developed which shows that growth is approximately exponential and is linearly related to food concentration. A random walk model reveals that the swimming process can be approximated as a simple diffusion term which, when included in the exponential growth model, leads to accumulation of consumers in high growth (=prey) areas. This diffusive migration of consumers up the prey gradient is rapid; for example, half- maximum growth is reached in <2 hours for fish larvae swimming in a 10 m patch of copepod nauplii. Enhancement of the net growth by this process is substantial; larval fish growth rates increase by 25% when 10 m prey patches appear at 5 hour intervals and by $>100\%$ for steady patches. Physical turbulence, at intermediate levels, causes patch dissipation and reduced growth, whereas, at higher levels, it causes growth to be restored to original, low-turbulence, values due to increased encounter velocities. Variations in population growth rate due to turbulence and micropatchiness, even when small ($<10\%$), can cause large fluctuations in recruitment by affecting duration of pre-recruit life.

1. Introduction

Pelagic marine ecosystem dynamics are the integrated result of myriad interactions occurring between individual organisms. The nature of this integration defines the time and space scales which are most important in driving system level processes. At present, little has been done to determine the potential significance of individual interactions to higher levels of organization, and there is confusion over which scales are most relevant, e.g., whether the scale of the individual is important in determining system level response to large scale physical forcings (Marine Zooplankton Colloquium, 1989). Understanding the process of integration from small to large scales requires knowledge of microscale (<10 m) distributions and behaviors and

1. Department of Biology, Woods Hole Oceanographic Institution, Woods Hole, Massachusetts, 02543, U.S.A.
2. Department of Earth, Atmospheric and Planetary Sciences, Massachusetts Institute of Technology, Cambridge, Massachusetts, 02139, U.S.A.

how these interact to control population and ecosystem dynamics. In particular, it is essential to know the extent to which microscale patchiness exists in the ocean and whether such aggregations are of any consequence to population growth and survival.

At present, models which predict population growth and distribution of marine zooplankton species rely on estimates of individual growth and reproductive rates derived from laboratory cultures. These same laboratory studies, however, have shown that food concentrations required for maximal growth and reproduction are often well above food levels found in the sea as determined with present sampling gear (eg. Reeve, 1980), suggesting that field animals may feed in micropatches too small to be sampled with traditinal gear and that such patches are of great importance in growth and recruitment of planktonic organisms (Lasker and Zweifel, 1978; Rothschild and Rooth, 1982). Workshops on ecology of fish larvae and zooplankton have repeatedly pointed out that the micro-fine scale environment is of critical importance to planktonic growth and survival (Fish Ecology III, Rothschild and Rooth, 1982; GLOBEC, 1988; Marine Zooplankton Colloquium, 1989).

Direct sampling of plankton distributions on scales <10 m is limited to the work of Owen (1981, 1989). Using a towed Nisken array, he found a large degree of contagion on scales <3 meters both horizontally and vertically. Microscale patchiness was found in a variety of environments under various wind conditions, patch amplitude and scale being inversely related to wind velocity. Sampling devices such as the LHPR (Haury and Wiebe, 1982), Batfish (Denman and Herman, 1978), and plankton pumps (Miller and Judkins, 1981) have poor resolution at scales <10 m due to spatial smearing problems, yet patchiness on large scales (10's of meters) is commonly found with these instruments suggesting that smaller scale patterns may be equally widespread. [Patchiness on still larger scales (hundreds of meters to a few kilometers), is, of course, well documented from closely spaced net tows, e.g. Sameoto (1978), Mackas and Anderson (1986)]. High frequency acoustical sampling also provides indirect evidence that zooplankton are heterogeneously distributed on the microscale (Pieper and Holliday, 1984). Methods of statistical analysis and some potential causes of small scale patchiness were reviewed in Fasham (1978) who pointed to the need for general theoretical models of patchiness. Despite empirical evidence and heuristic arguments for the existence and importance of microscale patchiness of plankton, little has been done to establish the theoretical framework in which organismal level processes translate to the population.

A primary factor controlling growth rate in plankton is the rate of encounter between consumer and prey. A recent analysis of the effects of turbulence on encounter rates shows clearly that the turbulent component of encounter velocity must be included in models of predator-prey interactions (Rothschild and Osborn, 1988). Encounter rates are much higher when this physical component is included as

opposed to only the swimming velocities of predator and prey (Gerrittsen and Strickler, 1977).

Although turbulence increases encounter velocity, it may at the same time reduce encounter rate due to dispersion of any existing predator-prey patches. Thus physical turbulence such as wind-induced mixing has a twofold effect: in a homogeneous environment, it will increase encounter rates, as shown by Rothschild and Osborn (1988), while, in a patchy environment, turbulent dissipation will reduce the rate to some unknown degree.

Given these considerations, we asked the following three questions: (1) Can microscale aggregations of predator and prey affect growth rate of planktonic populations? (2) Does turbulence increase or decrease growth rate? and (3) Are these changes in growth rate large enough to affect survival and recruitment?

The objective of this paper is to present results from a series of theoretical models, both analytical and numerical, which show that microscale patchiness can enhance planktonic growth rates, that turbulence, depending on its strength, will either enhance or reduce growth rates, and that even slight variations in growth rate cause large fluctuations in recruitment. The first model (Section 2) we develop describes the detailed dynamics of the growth of a single organism as it encounters prey. The prey are encountered randomly at a specified mean rate (to be determined in later sections as a function of the prey concentration, the swimming motion of the predator, and the turbulence). Components of the growth dynamics include ingestion, egestion, assimilation, respiration and excretion. The model predicts gut fullness and body weight through time. We show that growth is effectively exponential and is linearly related to food concentration so that patchy food supply leads to patchy growth rates. Comparison of the detailed model in the presence of fluctuating food supply to the exponential model gives reasonable agreement. Thus Section 2 gives a solid basis for subsequent use of the simple exponential growth model.

We then explore the role of swimming and patchy food supply on the growth of a predator. From a random walk model, we derive an appropriate form of a diffusion term and combine this with the variable growth model derived in Section 2. Enhancement of growth can be substantial when the patches of food persist long enough that the predators are able to swim into them; e.g., for 1 cm fish larvae swimming in a field of 10 m patches of nauplii which persist for only a few hours, we find a 25% enhancement to population growth. In Section 4, a general analysis of the growth/swimming equation shows the dependence upon the parameters and the patch structure. The enhancement to growth could be determined if the space-time spectrum of the prey were known. In subsequent examples, however, we consider only selected wavelengths and frequencies.

The effects of turbulence on the encounter rate and therefore the growth are discussed in Section 5. From this analysis, the growth enhancement, both from the swimming discussed previously and from the more frequent encounters associated

with the physical motions, can be compared to the dissipation of patchiness by the turbulent diffusion. At low levels of turbulence, growth rates are high because prey patches disperse slowly, and predators swim into these patches and feed at elevated rates. At intermediate levels, prey patches are dispersed rapidly and growth rate is reduced. At high levels, growth rate increases again, because turbulence enhances the encounter rate even though prey concentrations become homogeneous.

Finally, in Section 6, we analyze the relationship between growth rate, survival rate, and recruitment. Small changes in growth rates can cause large deviations in recruitment. Such growth changes are as significant to recruitment as are equivalent changes in mortality rate. The analyses presented in the paper apply over scales from centimeters to meters (eg. from copepods to fish larvae), and we assume food-limited conditions, since, otherwise, patchiness would not affect growth.

2. Individual growth model

To examine the degree to which an organism can buffer the effects of a patchy food environment we develop a generic mass transport model of growth and then derive parameter values using the copepod *Calanus pacificus* as an example. We develop this model from the components of growth to show that, under food limiting conditions, growth rate is directly proportional to food concentration and is approximately exponential over time scales relevant to micro-scale patchiness. Subsequent models use the simple exponential approximation. While it is necessary to justify this simplification by developing the full growth model, an understanding of the latter is not essential to our analyses in subsequent sections of the interactions between swimming, patchiness, and turbulence.

a. Organismal model. In this section, we construct a model for the response of a consumer to a source of food. We focus on individual encounters with prey organisms and the probability of ingestion given the amount of food in the gut and the body mass of the consumer.

We consider the flow of food energy (or mass) through a predator (or herbivore) (Fig. 1); the terms in boxes represent the amount of mass in the gut (G), in body tissue (T), in storage (S), and in a labile fraction (L), while the rest of the symbols represent rates of mass flow between various compartments (see Appendix). A food source F (mass per unit time "arriving" at the predator) is ingested I into the gut G and is assimilated A into a labile fraction L or egested Eg. The labile fraction is lost to respiration and excretion RE with any excess put into storage S and/or body tissues T. The standard definition of growth rate (change in body weight with time, Dw/Dt) includes both changes in body tissue T (i.e., tissue growth rate, TG) as well as changes in storage S (i.e., DS). Although assimilated materials may be incorporated

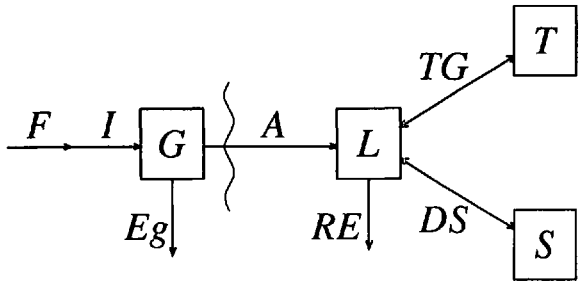

Figure 1. Schematic of model for individual consumer growth. F = food source (mass per unit time "arriving" at the consumer), I = ingestion rate, G = food mass in gut, E = egestion rate, A = assimilation rate, L = labile fraction, RE = respiration/excretion rate, TG = tissue growth rate, T = tissue, DS = storage rate, S = storage. Growth rate is defined in this system as $(TG + DS)$ or the change in $(T + S)$ with time.

into tissues or storage at relatively different rates, depending on metabolic needs and available food, we consider growth rate as the sum of TG and DS. Growth rate, therefore, is simply the difference between rates of assimilation A and respiration plus excretion RE (Fig. 1). Note that this formulation allows for negative growth if respiration plus excretion is greater than assimilation.

We begin with a stochastic model for individual prey particles encountered by the predator. Once we understand the dependence of an organism's growth rate on the rate at which it encounters food particles, we can begin modeling the effect of patchiness which makes the "arrival" rate vary in space and time. We define the encounter rate E as the average number of particles the predator encounters per unit time:

$$E = \frac{C\mathscr{F}}{\overline{M}}$$

where C is the average food concentration (mass/volume), $\mathscr{F}$ the average foraging/filtering rate (volume/time), and $\overline{M}$ the average mass of a particle. Food particles considered are those of a size which the predator is capable of ingesting. The foraging/filtering rate, $\mathscr{F}$, depends on the predator's swimming and perceptive radius, the prey's movement (which is relatively small), and the level of turbulence. It is the interaction between these factors that transforms spatial patchiness into temporal variations in prey encounter.

We first represent particle mass and interval between encounters as random variables, and then simplify the model by averaging over many arrivals, assuming that they occur rapidly compared to the time scales of the predator's growth dynamics (Fig. 1). The mass of food arriving within range of the predator per unit time, $F(t)$, can be modeled in terms of individual food particles appearing in a random series

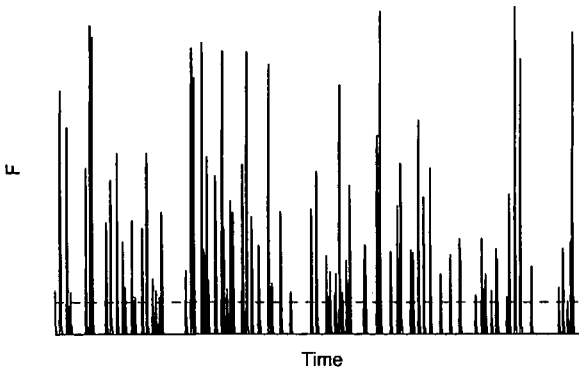

Figure 2. Random time series of individual food particles encountered by a consumer. Food, F, is mass per unit time "arriving" at the predator. Area under each Gaussian spike corresponds to the mass an individual prey. Width of each spike corresponds to handling time, τ, of the prey, which may be ingested or rejected depending on gut fullness. Since τ is small relative to time between encounters, each spike approximates a Dirac delta function. In addition, particles arrive rapidly relative to the consumer's growth rate so that this statistical representation can be converted to a deterministic one giving the expected value for arrival rate of food mass. Arrival rate is dependent on particle size distribution as well as on body size of predator.

(see Fig. 2):

$$F(t) = \sum M_i \mathcal{G}(t - t_i)$$
$$\equiv \sum M_i \frac{1}{\sqrt{\tau\pi}} \exp\left(\frac{-(t - t_i)^2}{\tau^2}\right) \tag{2.1}$$

where t is time, M_i is the mass of the i^{th} food particle (in chronological order), t_i is the time at which it arrives, τ is the handling time, and $\mathcal{G}$ is the Gaussian function. Thus, each food particle is represented as a single Gaussian pulse, the sum of these pulses giving the function $F(t)$. The integral of $\mathcal{G}$ is one, so that the net mass (the integral of F) for a single encounter is indeed M_i. The function $F(t)$, shown graphically in Figure 2, appears as a random series of spikes which correspond in area and temporal spacing to individual particle mass and arrival time, respectively. In the limit as τ becomes very small, $\mathcal{G}$ becomes a Dirac delta function. To construct a realization of $F(t)$ we need to specify the distribution of masses, M_i, and arrival times, t_i, which are both random variables. In the field, particle frequency decreases with increasing diameter according to the well known Sheldon spectrum (Sheldon *et al.,* 1972; Platt and Denman, 1978)—the biomass in each octave is the same. Therefore the probability distribution function $\mathcal{P}(M)$ must satisfy

$$\int_M^{2M} M'\mathcal{P}(M')\,dM' \text{ is independent of } M.$$

This will occur when the indefinite integral is a log, so that the definite integral

depends only on the ratio of the limits. Therefore the probability of finding a particle with mass between M and $M + dM$ is proportional to dM/M^2.

For arrival times, we use the following argument. If the particles are randomly scattered in space with a uniform distribution (on the relevant subpatch scales) and the foraging rate is constant, the arrival times will also have a uniform random distribution. The time between arrivals then has a known distribution (Stevens, 1939) characterized by the mean, which is simply the inverse of the average encounter rate, E:

$$\langle t_{i+1} - t_i \rangle = 1/E. \tag{2.2}$$

To a reasonable approximation (Newall, 1963), the probability of an arrival interval being in the range τ to $\tau + d\tau$ is just an exponential distribution, $E \exp(-E\tau)d\tau$.

As the animal grows, however, it moves through the spatial array of prey more rapidly, so that the encounter rate increases (and therefore the mean time between arrivals decreases). This is reflected in the variation of the foraging rate, $\mathcal{F}$, with predator weight. Foraging volume is taken to be a power function of the organism's weight w (eg. Huntley and Boyd, 1984). Let w_0 be the initial weight at time $t = 0$ and E_0 be the rate at which organisms of that weight encounter food particles when the food concentration is C_0. Then we take

$$E = \left(\frac{w}{w_0}\right)^m \left(\frac{C}{C_0}\right) E_0. \tag{2.3}$$

The weight dependence ($m > 0$) represents the fact that larger animals can forage/filter larger volumes. From food concentration, turbulence (which alters the factor E_0), and the predator's foraging rate, we can estimate the encounter rate E. Note that this rate is for encountering particles of any size within the range which the predator can eat. Next, we shall consider the probability that a particle is ingested, given the particle mass and the body weight and gut mass of the predator.

We shall take the probability that an encountered particle of mass M will be ingested to be

$$F_i(a_+[w/w_0]^s - G - M)$$

where G is the current gut mass and $a_+(w/w_0)^s$ is the maximum possible gut mass at the current body weight. (The constant a_+ is thus the maximum gut mass for an organism of weight w_0.) The function F_i will be zero when its argument is negative (predator too full to ingest particle) and approaches unity when its argument becomes positive enough. The simplest form is just a step function, but smoother functions could also be considered.

b. Average growth of a predator. We could design a stochastic simulation to generate the next arrival time and particle mass, given the current predator weight, and then

we could decide randomly whether or not the particle is ingested given the current mass in the gut G and the probability function F_i. However if the particles arrive frequently enough compared to the biological times scales, it is useful to convert the statistical model into a deterministic one.

We can calculate the expected value of the ingested mass per unit time:

$$I = E_0 \left(\frac{w}{w_0}\right)^m \left(\frac{C}{C_0}\right) \int \alpha \frac{dM}{M} F_i(a_+[w/w_0]^s - G - M)$$

where the constant α can be found by choosing the rate of ingestion I_0 for organisms of weight w_0 which have empty guts $G = 0$ and which are feeding at food concentration C_0. If we use a step function form for F_i, we can carry out the integral above to find

$$I = I_0 \left(\frac{w}{w_0}\right)^m \left(\frac{C}{C_0}\right) \frac{\ln (a_+[w/w_0]^s - G) - \ln (M_{\min})}{\ln (a_+) - \ln (M_{\min})} \tag{2.4}$$

with $\alpha = I_0/E_0$ and $M_{\min}$ is the lower limit on the prey that the predator will ingest. This expression simplifies considerably in the case where the powers s and m are identical and where $M_{\min}$ scales as $a_-(w/w_0)^m$ (which implies that the ratio of maximum prey mass to minimum prey mass a_+/a_- is fixed over the predator's planktonic life). The constant a_- is the minimum particle mass ingested by a predator of mass w_0. Then (2.4) becomes

$$I = I_0 \left(\frac{w}{w_0}\right)^m \left(\frac{C}{C_0}\right) \frac{\ln (a_+ - G/[w/w_0]^m) - \ln (a_-)}{\ln (a_+) - \ln (a_-)}. \tag{2.5}$$

It is possible to make similar arguments in the case of other forms of F_i as well; we find that ingestion depends only on $G/(w/w_0)^m$ when the prey masses span a fixed ratio. As shown below, this leads to familiar looking ingestion versus food concentration curves when the gut is in equilibrium.

If we now let rates of assimilation and egestion be proportional to mass of food in the gut, G, we have

$$A = a_e a_g G \tag{2.6}$$

$$Eg = (1 - a_e) a_g G \tag{2.7}$$

where a_g is rate of gut evacuation, and a_e is the fraction of food lost from the gut by assimilation. When the gut is in equilibrium (so that $I = A + Eg$), a_e corresponds to the assimilation efficiency (A/I).

At a given fixed temperature, the weight-dependent respiration plus excretion is

given by

$$RE = a_r(w/w_0)^n \tag{2.8}$$

where a_r (the rate for an organism of weight w_0) and n are found from experimental observation. Combining equations (2.5–2.8) gives the general equations for growth

$$\frac{Dw}{Dt} = A - RE = a_e a_g G - a_r(w/w_0)^n \tag{2.9}$$

$$\frac{DG}{Dt} = I - Eg - A = I_0\left(\frac{w}{w_0}\right)^m\left(\frac{C}{C_0}\right)\frac{\ln(a_+ - G/[w/w_0]^m) - \ln(a_-)}{\ln(a_+) - \ln(a_-)} - a_g G. \tag{2.10}$$

Although this growth formulation does not include ingestion-dependent assimilation efficiency or respiration (specific dynamic action), these effects are expected to be small. Most ingestion-dependent respiration is due to specific dynamic action (Kiorboe, 1985; Lampert, 1986) which scales with assimilation. When variations in gut mass are small, this effect can be included as a constant in the assimilation term and is therefore independent of patchiness. Likewise, variations in assimilation efficiency (±10%; Landry *et al.,* 1984) are small relative to 2–3 fold changes in food concentrations commonly observed in the field and used in the present model. Preliminary calculations have shown that ingestion-dependent assimilation efficiency has little effect on growth rate response to patchy food.

c. Solutions. Finally, we look at solutions to our model (2.9–10) and examine the dependence of the growth rate on food concentration. These calculations indicate that a simple exponential model, with the growth rate proportional to food concentration, is a reasonable approximation to the full growth model.

In the Appendix, we solve these equations in the special case where m and n are both one and (2.9-10) can be linearized. This derivation shows that body weight grows exponentially and that the growth rate is nearly proportional to the food concentration C. In addition, we remark that, when the gut is in equilibrium, we can neglect the left-hand side of (2.10), yielding

$$I/(w/w_0)^m = a_g\hat{G} = I_0\left(\frac{C}{C_0}\right)\frac{\ln(a_+ - \hat{G}) - \ln(a_-)}{\ln(a_+) - \ln(a_-)}$$

where $\hat{G} = G/(w/w_0)^m$. We can use the left hand equality to eliminate $\hat{G}$ on the right-hand side, thereby obtaining a single relationship between the ingestion, I, and the food concentration, C, as plotted in Figure 3. In equilibrium, ingestion depends on food concentration in a fashion similar to Ivlev's (1955) model: the saturation stems from the decrease in ingestion when the mass of food in the gut becomes too large compared to the weight of the organism. A good fit to the Ivlev curve is

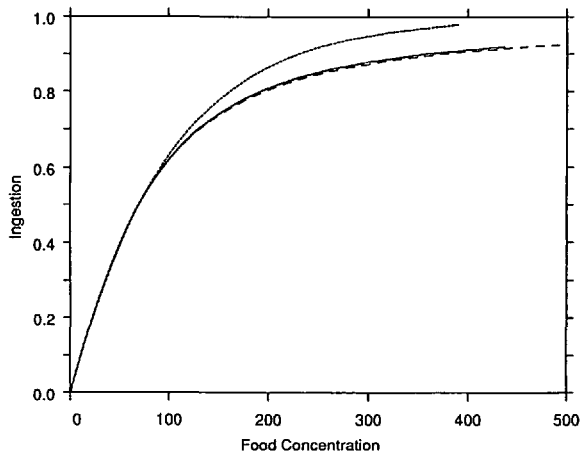

Figure 3. Ingestion rate (mass/time) versus food concentration (mass/volume) as determined from equation (2.10) of the individual growth model with the gut in equilibrium (i.e., $DG/Dt = 0$). The model was parameterized for *Calanus pacificus*. Size distribution of available food particle mass was assumed to follow the Sheldon spectrum (solid curve) with uniform mass (zero slope) as a function of size (octave scale) as well as the theoretical model of Platt and Denman (1978) (long dash) with the slope = −0.22. Shown for comparison is Ivlev's (1955) curve parameterized for *C. pacicifus* (short dash). Saturation is due to increasing gut fullness at higher food levels.

obtained if we match the saturation value, $I/(w/w_0)^m$, the slope at the origin, and the value of food concentration at half-saturation. The latter implies that $a_-/a_+ = 0.129$, so that the organisms are ingesting food particles with about an order of magnitude range in mass. Note that the choices of $s = m$ and the form of $M_{\min}$ come from the indications that the slope and saturation value both scale as $(w/w_0)^m$ and that the half saturation value of food concentration is independent of the predator's weight. Of course the evidence for these is much less certain than the general shape of the ingestion curve; we do not believe that our conclusions depend significantly upon the exact assumptions.

For the case when m and n are unequal and less than one, we solved the equations numerically to show that growth is nearly exponential, with the rate proportional to food concentration. Parameters values were estimated from the data of Vidal (1980) for *Calanus pacificus* grown at 12°C (all units are based on μg carbon and days). Respiration values are $a_r = 0.42$ and $n = 0.82$. The exponent for the dependence of foraging and also of maximum gut fullness on weight was $m = 0.77$. The gut evacuation rate, $a_g = 55.3$, is based on a clearance (90% loss) time of one hour (Marshall and Orr, 1955), and assimilation efficiency a_e was taken to be 0.75 (Landry *et al.*, 1984). Food concentrations were in the limiting range (50–150 μgC/l). Vidal's data for maximum ingestion rate (saturating food) were used to derive the coefficients $I_0 = 1.607$ and $a_+ = 0.0334$. Figure 4 shows the log of the weight versus time for various food concentrations. The near linear nature of the curves indicates that

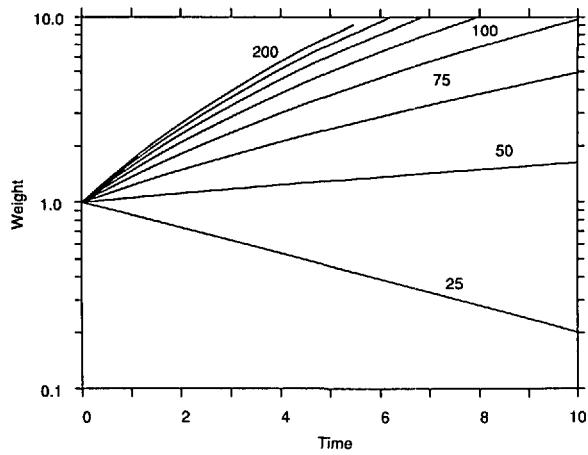

Figure 4. Change in body weight (μgC) versus time (d) of *Calanus pacificus* as determined from the individual growth model (equations 2.9–2.10) assuming exponents for weight-dependent filtration and respiration rates are unequal and less than one. The curves of $\log_{10}$ (weight) vs. time at different food levels (μgC/l) are nearly linear showing that growth is approximately exponential in this limiting range of food (see Fig. 3).

growth is approximately exponential. When there is not enough food, the weight decreases. When the concentration reaches a critical value, the organism can maintain a steady weight; above this, growth is positive. We estimate a growth rate over the time period indicated on Figure 4 and plot it as a function of food concentration C in Figure 5. The growth rate saturates at high food concentrations (>200 μgC/l) and has a roughly linear dependence on food in the relevant range, (50–150 μgC/l).

As a particular example, we present in Figure 6 a detailed solution of (2.9–10) using a time-varying food concentration $C = 100 + 50 \cos(2\pi t/1 \text{ day})$ μgC/l. This is compared to a solution of

$$\frac{DB}{Dt} = g(C)B \tag{2.11}$$

with $g(C)$ being the particular linear functions of C shown in Figure 5 (dashed lines). The weight histories are very similar. Thus a fairly simple exponential model gives a reasonable representation of the growth, and we shall use it in subsequent sections. Next we shall include additional terms in Eq. (2.11) to account for the organism's movement.

3. Swimming diffusion and growth of predator

The combined effects of swimming, physical turbulence, and patchy individual growth rate on predator population growth were explored in stepwise fashion. In this section, a diffusion term for predator swimming is derived from a random walk

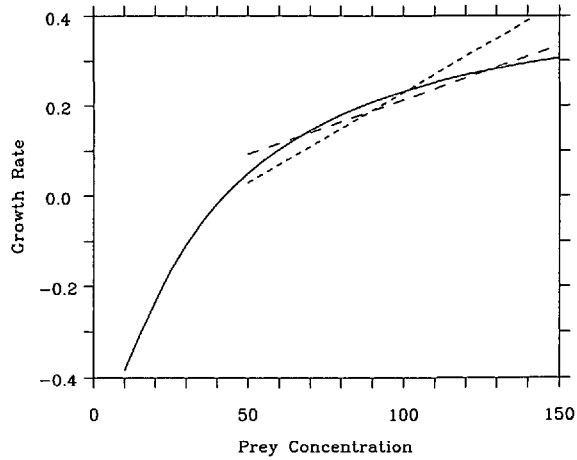

Figure 5. Growth rate over the 10 d period shown in Figure 4 as a function of food concentration, C (μgC/l) as determined using the individual growth model (solid). The two dashed lines show linear relationships between food and growth which are used in the exponential model, Eq. (2.11). The long dashed line is a least squares fit over the range 50–150 μgC/l while the short dashed line is chosen to represent the details of the growth shown in Figure 6 over the whole period. They are different because the growth rate is somewhat sensitive to weight; the lines in Figure 4 are not truly straight.

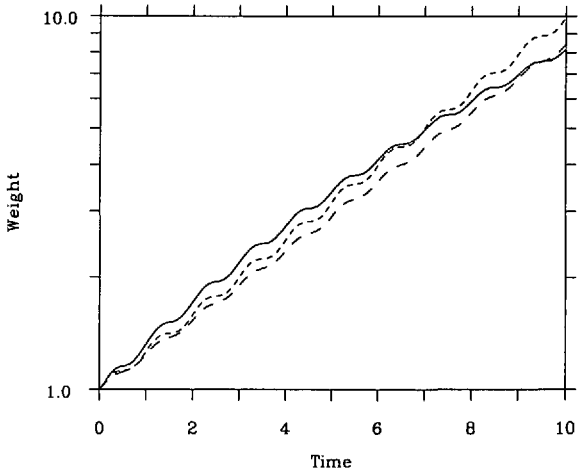

Figure 6. Body weight (μgC) versus time (d) for exponential (dashes, corresponding to the lines in Fig. 5) and full growth (solid) models. Food concentration fluctuates as a cosine function in the limiting range (50–150 μgC/l) with a period of one day. The exponential models, with growth rate a simple linear function of food concentration, can closely approximate the more complex full growth model.

model, and a basic equation relating growth and swimming diffusion is given together with an example of the interaction between these variables. A general analysis of the basic equation follows (Section 4) showing the relationship between swimming, growth, and patch spatial structure. Finally (Section 5), the equation is expanded to include the turbulent component of the encounter velocity so that the magnitude of this effect can be gauged against turbulent dissipation of the patchiness. The latter form of the equation was solved numerically for selected cases.

a. Swimming diffusion. It is necessary to understand the difference between swimming and physical diffusion processes. For swimming behavior, the diffusion equation takes the form

$$\frac{\partial}{\partial t} B = \frac{\partial}{\partial x} \kappa_1 \frac{\partial}{\partial x} \kappa_2 B \tag{3.1}$$

rather than the more familiar parameterization

$$\frac{\partial}{\partial t} B = \frac{\partial}{\partial x} \kappa_1 \frac{\partial}{\partial x} B \tag{3.2}$$

for physical diffusion. This distinction is a very important factor in both the local and the net enhancement of growth associated with patchy food: biomass accumulates in regions where κ_2 is small while variations in κ_1 affect the spreading rate but do not give accumulation. Okubo (1980) discusses various forms leading to (3.1) with constant κ_1 using random jumps between prey where the concentration of prey varies. Here we shall derive a form like (3.1) from a more realistic model of foraging which explicitly includes the swimming velocity required for the predator to move from place to place.

Let us divide the population biomass into three groups, one moving left, one right, and one which is stopped, with biomasses b_l, b_r, and b_0, respectively. We define transition rates (which depend on prey density) between these three states. Then we have equations for time changes in each of the biomass groups:

$$\frac{\partial}{\partial t} b_l = \frac{\partial}{\partial x} (v b_l) - (T + S) b_l + T b_r + \frac{R}{2} b_0 \tag{3.3}$$

$$\frac{\partial}{\partial t} b_r = -\frac{\partial}{\partial x} (v b_r) - (T + S) b_r + T b_l + \frac{R}{2} b_0 \tag{3.4}$$

$$\frac{\partial}{\partial t} b_0 = S b_l + S b_r - R b_0 \tag{3.5}$$

where T is the rate of turning without stopping, S is the rate of stopping, and R is the rate of starting from a stopped state. Notice that we have assumed a number of

symmetries: for example, predators starting to move will go with equal probability in either direction and turning/stopping rates are independent of the direction of movement. The swimming rate v is assumed to be the same in either direction, although it may vary spatially. We can rewrite these equations in terms of the biomasses at any point $B(x, t) = b_l + b_r + b_0$ and the net rightward moving biomass $B_r = b_r - b_l$ as

$$\frac{\partial}{\partial t} B = -\frac{\partial}{\partial x} (vB_r) \tag{3.6}$$

$$\frac{\partial}{\partial t} B_r = -\frac{\partial}{\partial x} [v(B - b_0)] - (2T + S)B_r \tag{3.7}$$

$$\frac{\partial}{\partial t} b_0 = SB - (S + R)b_0. \tag{3.8}$$

Let us first look at the steady-state solutions to this model. Eqs. (3.6–8) have steady solutions when $B_r = 0$ and $v(B - b_0)$ is constant since B, B_r, and therefore b_0 are then constant in time. Using these criteria we find

$$B = \frac{S + R}{vR} \text{const.} \tag{3.9}$$

(where the constant is $v(B - b_0)$). This equation implies that predators accumulate in regions with high prey density, since these are regions in which one would expect the rate of stopping, S, to be high and the rate of starting, R, to be low. It is also possible that the swimming rate v decreases in higher food areas (Hunter and Thomas, 1974).

Note that the rate of turning (without stopping), T, does not enter into the expression (3.9) for accumulation of biomass. An independent random-walk model which we developed for an organism swmimming through a patchy prey field confirms that the process of turning more rapidly in high prey regions only affects the spreading rate but does not lead to final accumulation. Rather the time spent in reduced swimming or in handling prey (and not swimming) determines the accumulation.

We now consider the time-dependent evolution of $B(x, t)$ and show that it is the rates of stopping, starting, and swimming which determine κ_2 (Eq. 3.1), whereas rate of turning affects only κ_1. We shall assume that the time scale for motion through a patch (length scale/v) is long compared to the time scales for starting ($1/R$), stopping ($1/S$), and turning ($1/T$). In that case equations (3.7–3.8) are always in quasi-equilibrium so that

$$b_0 = \frac{S}{S + R} B$$

and

$$B_t = -\frac{1}{2T+S}\frac{\partial}{\partial x}\left[\frac{vR}{S+R}B\right]$$

with the biomass evolving according to

$$\frac{\partial}{\partial t}B = \frac{\partial}{\partial x}\left[\left(\frac{v}{2T+S}\right)\frac{\partial}{\partial x}\left(\frac{vR}{S+R}\right)B\right]. \tag{3.10}$$

Eq. (3.10) is identical in form with (3.1) if we identify

$$\kappa_1 = \frac{v}{2T+S} \quad \text{and} \quad \kappa_2 = \frac{vR}{S+R}.$$

As stated above, we anticipate that in regions of high prey density the predator is more likely to stop and less likely to start swimming. Furthermore, since more time is spent stopped, less will be spent turning without stopping. This would imply that T and R decrease with increasing prey density while S increases. This is the simplest, conservative, assumption, i.e., that predators have no memory but remain in high prey areas longer simply because more time is spent capturing and handling prey. In addition, as mentioned above, predators may actively modify their swimming speed according to prey density such that in high prey regions v also decreases (Hunter and Thomas, 1974). Therefore κ_2 will decrease with increasing prey concentration, while the changes in κ_1 may be of either sign. (One could imagine other scenarios especially with respect to T, but one would still expect κ_2 to behave similarly as long as the stopping/starting process depends on prey concentration.) For maximum simplicity, we make the choice that $2T + S$ and v are constant, equivalent to the hypothesis that the total *net* rate of turning, including both turning without stopping and stopping and restarting in the opposite direction, is fixed. This makes κ_1 a constant (chosen to be one) while

$$\kappa = \frac{v^2R}{(2T+S)(S+R)}$$

and varies inversely as the encounter rate. In this case, when $\kappa_1 = 1$, we shall drop the subscript on κ_2.

The form (3.1) with the second spatial derivative of diffusivity allows predator biomass to gather in areas of high prey concentrations even without actual growth. The variable κ_2 in Eq. (3.1) is permitted for "biological" diffusion caused by random swimming of organisms because of the "compressibility" of population biomass. In physical diffusion, the constraint of volume conservation requires that only κ_1 be variable. In a sense, fluid particles only turn but do not stop. With the present formulation, which for now considers only biology, predators will diffuse out of areas of high "swimming diffusion," κ, and into areas of low swimming diffusion.

b. Swimming diffusion and growth. In Section 2, we found that growth rate in fluctuating food was approximately exponential and proportional to food concentration so that patchy food supply translates directly into patchy growth rate. We now explore the interactive effects of patchy growth rate and swimming on predator population growth using an equation of the form

$$\frac{\partial}{\partial t}B = gB + \frac{\partial^2}{\partial x^2}(\kappa B) \tag{3.11}$$

where $B(x, t)$ is the biomass of the population at time t at a point x in a one dimensional domain, $g(x, t)$ is the weight-specific growth rate of B at (x, t), and $\kappa(x, t)$ is the diffusion rate of B at (x, t) due to the swimming behavior of the predators. Predator population biomass, B, can be considered as an ensemble average over many growth (= prey) patches and many predators. To illustrate the nature of the basic mechanisms involved, we choose an example in which the growth rate g varies in time and space according to

$$g = b - a\cos(kx - \omega t) \tag{3.12}$$

where a, b, and ω are chosen to simulate the effects of patchy prey on predator growth rates found using the individual growth model discussed above. From Section 2, we can assume that growth is exponential, approximating the growth curve derived from Eqs. (2.9–10). This is a common form for zooplankton (e.g., Huntley and Boyd, 1984, copepods; Bolz and Lough, 1983, cod and haddock larvae). The diffusion coefficient, κ, includes a mean diffusivity K_0 together with a space and time dependent diffusion term due to variable predator swimming and food handling

$$\kappa = K_0 + K_2\cos(kx - \omega t) \tag{3.13}$$

where K_2 is the maximum variation in diffusion due to variations in swimming. By choosing $a > 0$ in Eq. (3.12), the diffusivity (Eq. 3.13) is highest where growth rate (prey concentration) is lowest. As discussed above, this can be associated with lower stopping rates S or increased swimming velocity v in areas of low growth. Conversely, in areas where prey concentrations are highest, predators diffuse at only background rates $K_0 - K_2$; this is due to residual swimming at high prey densities. Substituting equations (3.12 and 3.13) into (3.11) gives

$$\frac{\partial}{\partial t}B = [b - a\cos(kx - \omega t)]B + \frac{\partial^2}{\partial x^2}[K_0 + K_2\cos(kx - \omega t)]. \tag{3.14}$$

For illustrative purposes, parameter values are chosen for Eq. (3.14) to approximate growth and swimming of a 1.0 cm haddock larva feeding in a 10 m (wavelength) patch of copepod nauplii. Haddock growth, g, has a minimal value of -0.05 and a maximum of 0.15 (cf. Laurence, 1985b). Values of K_0 and K_2 are more difficult to estimate. For random swimming by a larva we take velocities up to 1.5 body lengths per second

(1.5 cm/s) in the low prey region to 0.5 cm/s in high prey regions (Laurence, 1985a; Hunter and Thomas, 1974; Munk and Kiorboe, 1985). Given a perceptive field of 1.0 cm^2, a range of prey concentrations of 10–100/liter gives times between prey encounters ranging from 67–20 seconds. We can use this to estimate a rate of stopping as the inverse of these times; if we then assume that the handling time, and therefore R is fixed, we find the ratio of diffusivities to be

$$\frac{K_0 + K_2}{K_0 - K_2} = \frac{1.5^2}{0.5^2}\left(\frac{R + 10/200}{R + 3/200}\right).$$

It can be seen from this expression that even a relatively short handling time, $1/R$, (4/3 seconds) causes the diffusivity to vary by a factor of 10. If we take this factor as a conservative estimate for variation in swimming diffusion, we can estimate a maximum diffusivity $K_0 + K_2$ by assuming that the predators will turn within 10 cm (i.e., 10 body lengths) in the absence of prey, i.e., $K_0 + K_2 = 10$ cm^2/s.

A similar range in diffusivity is found using Okubo's (1980) expression

$$\kappa = \tfrac{1}{2}vl$$

where v is the swimming speed and l is mean free path. If we let l equal 0.1 × distance between prey (i.e., 10–1 cm), κ ranges between 7.5–0.75 cm^2/s.

Eq. (3.14) was solved numerically, and spatially averaged population growth was computed through time. A fully implicit numerical scheme (Roache, 1982) was used together with periodic boundary conditions. Numerical stability was checked by reducing the time step. Accuracy of the scheme was confirmed via comparison with analytical solution of 1-D advection diffusion of a scalar and with the two-step explicit method discussed in Davis (1984a). Time units are in days and space was nondimensionalized with a domain size of 2π radians.

Several parameterizations of this spatial model were used to examine the effects of patchy individual growth rate on population growth. Initially, to observe the effects of only spatial variation in growth g (i.e., no swimming), the parameters ω, K_0, and K_2 were set equal to zero. With a uniform initial distribution of predators (i.e., $B(x, 0) = 1.0$), the population was allowed to grow to near steady state at $t = 100$ d (Fig. 7). The analytical solution to this simple case gives a steady state population growth rate of 0.15/d which is closely approximated numerically (Fig. 7A). The relative spatial distribution of biomass within the domain approaches a delta function (all biomass at a single point) at $x = \pi$ as t approaches infinity (Fig. 7B). This occurs simply because biomass grows most rapidly at patch center. Background (spatially uniform) diffusion, set to the minimum value $\kappa = K_0 - K_2$, by itself (i.e., when $\omega = 0$) causes a reduction in maximal growth rate with increasing κ and smooths out the spatial distribution of B from that shown in Fig. 7B. Note that only predators are diffused in this case since κ is due to uniform swimming by predators, and that the prey (i.e., growth rate) patch is fixed since $\omega = 0.0$.

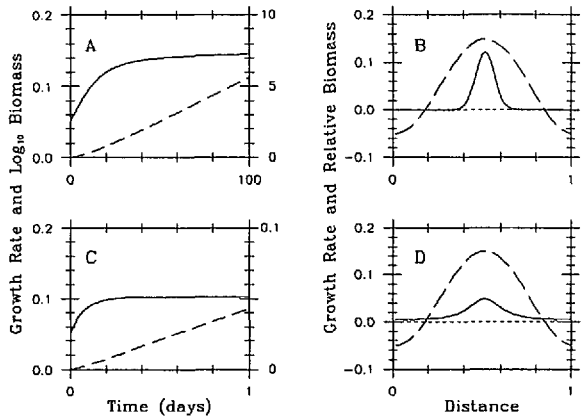

Figure 7. Effects of patchy individual growth rate (∝ food concentration) on population growth when patchiness is time invariant. Left panels (A and C) show spatially averaged weight-specific growth rate (/d) (solid) and ln of body weight (dash) vs. time. Right panels (B and *D*) show weight-specific growth rate (long dash) and biomass distribution (solid) vs distance (domain size normalized to one) at t = 100 d (i.e., near steady-state). Growth without and with predator swimming are shown in top (A–B) and bottom (C–D) panels, respectively (note scale changes in A and C). Growth rate outside and inside patch is −.05 and 0.15 (/d), respectively (panels B and D, dashed curve). Model can apply to a 1.0 cm fish larvae swimming in a 10 m (wavelength) patch of copepod nauplii (10–100/liter) or to a 1 mm adult copepod swimming in a 1 m patch of algal cells (10^4–10^5/liter).

Spatially variable swimming within the domain causes the maximal population growth to be reached much faster (Fig. 7C). The population at 100 d is less restricted to the regions of highest growth due to background diffusion (Fig. 7D). In this example, the previously derived range in diffusivity was used, 1–10 cm^2/s, which is representative of a 1 cm fish larvae swimming in a 10 m domain. Using these values, the larva enters the patch quite rapidly, attaining half-maximal growth in less than 2 hr, but maximal growth is reduced (0.1/d) due to background swimming diffusion (1 cm^2/s).

To demonstrate the potential effects of transient prey patchiness on predator growth we let $\omega = 2\pi$, corresponding to a patch translating through the domain once per day. Diffusion rates are 0.75–7.5 cm^2/s assuming a domain size of 10 m. The steady state specific growth rate (0.09/d) is a significant enhancement above the mean (nonpatchy) value of 0.05/d, an increase in specific growth rate of 80% (Fig. 8). If prey patches are more transient than one cycle per day, the enhancement of specific growth is less pronounced but still important. For example if a 10 m patch appears every 6 h, i.e., $\omega = 8\pi$ and κ = 0.75–7.5 cm^2/s, the enhancement in growth is 20% above the mean. Although this increase may not seem important, we show below that variations in specific growth rate of only 15% from one cohort to another can lead to order-of-magnitude variations in recruitment.

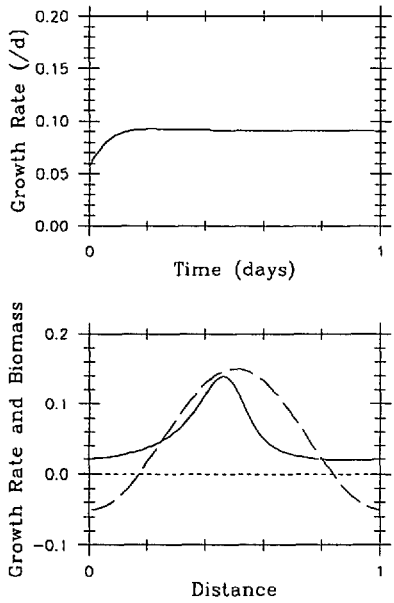

Figure 8. Effects of transient patchiness in growth rate on predator population growth. Top panel show weight specific growth rate (/d) of total population vs. time (d). Bottom panel shows steady-state (t = 10 d) spatial distributions of specific growth rate (dashed) and biomass (solid). Patches translate through the domain at one cycle per day.

Interactions between growth, swimming, and patch size and spatial structure are examined in detail in the next section, but immediate insights can be gained from the examples just presented. Swimming variation has a much greater effect on enhancement of population growth than does growth rate variation since the time scales for the latter effect are long (Fig. 7), i.e., biomass accumulates in the center of the patch more rapidly due to swimming than differential growth. Since we nondimensionalized space, the model applies over a range of dimensional scales, provided all length parameters scale with domain size. Thus the example of a 1.0 cm fish larva in a 10 m domain may also apply to a 1.0 mm copepod in a 1.0 m domain. In the latter case, the distance between prey encounters is 1–10 cm (l = 0.1–1.0 cm), and, if encounter radius scales with body length, the prey concentrations would be 10^4–10^5/liter which are reasonable densities for prey of a 1.0 mm copepod (i.e., algae and protozoans). A further implication of the nondimensional spatial scale is that increasing the number of patches in the domain (i.e., higher wavenumber) has the same effect as reducing the domain size but keeping a single patch. A simple cosine representation for patch structure (Eq. 3.14) provides insights into effects of patchiness on growth, however, scale-dependent effects can be important: more complex patch patterns are discussed below in relation to mean and variance of their Fourier spectra.

4. General analysis of predator equation

We now present some analytical results on the expected enhancement of predator population growth rate due to variable growth and swimming diffusion.

a. General equation. The predator Eq. (3.11) can be rewritten in general form as

$$\frac{\partial}{\partial t} B = [g_0(t) + g'(x, t)]B + \frac{\partial}{\partial x} \kappa_1 \frac{\partial}{\partial x} [K_0 + \kappa'(x, t)]B$$

where the terms g_0, K_0 and g', κ' are means and deviations in growth and diffusion, respectively, g' and κ' having no net spatial average. We can eliminate the mean growth term g_0 by defining

$$B(x, t) = b(x, t) \exp \left(\int^t dt' g_0(t')\right)$$

which removes the growth which would occur in the absence of any patchiness in prey. We then focus on the coefficient $b(x, t)$, which represents the predator biomass normalized by the biomass which would exist in the absence of prey patchiness. Our goal is to determine whether there is a component of $b(x, t)$ which has a nonzero spatial average and which grows in time; this component represents enhancement in the net growth associated with patchiness. The normalized biomass satisfies the equation

$$\begin{aligned} \frac{\partial}{\partial t} b &= g'(x, t)b + \frac{\partial}{\partial x} \kappa_1 \frac{\partial}{\partial x} \kappa_2 b \\ &= g'(x, t)b + \frac{\partial}{\partial x} \kappa_1 \frac{\partial}{\partial x} [K_0 + \kappa'(x, t)]b \end{aligned} \tag{4.1}$$

b. Steady case. When the prey distribution is fixed in space and time, so that $g'(x)$, κ_1, and κ_2 are independent of t, the predator distribution, as shown in Figure 9, settles into a pattern with highest concentration in the regions of high prey. The pattern scales exponentially with time; in other words, b is dominated by the most rapidly growing eigenfunction and the enhancement to the growth rate is the eigenvalue. To find these, we substitute

$$b(x, t) = \frac{\psi(x)}{\kappa_2(x)} \exp(\sigma t) \tag{4.2}$$

in (4.1), where σ is the enhancement in the growth rate associated with the prey patchiness. If we scale the eigenfunction ψ so that the spatial average of ψ/κ_2 is one, then it is clear that the spatially averaged B grows at a rate $\int g_0 + \sigma$ from an initial value of one. The choice of denominator in (4.2) comes from the form of b in the case without growth. Eq. (4.2), together with the condition that ψ be periodic on the

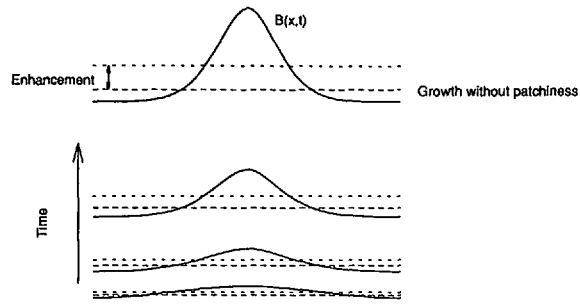

Figure 9. Spatial distribution of biomass at different times as determined with the predator growth equation. Biomass, B, grows exponentially at all locations but does so most rapidly at patch center. Factoring out the mean exponential growth (that which would occur in the absence of any patchiness), shown by the long dashes, removes a large part of the biomass increase. The relative spatial distribution of the biomass is determined by the most rapidly growing eigenfunction and the spatially averaged value of the biomass, indicated by the short dashes, grows at a more rapid rate than the biomass in the absence of patchiness. The enhancement in growth rate, σ, is the eigenvalue corresponding to the most rapidly growing eigenfunction.

domain $[0, L]$, gives the eigenvalue equation for σ

$$\frac{\partial}{\partial x}\kappa_1\frac{\partial}{\partial x}\psi = \frac{\sigma - g'(x)}{\kappa_2(x)}\psi. \tag{4.3}$$

We shall solve this numerically; however, it is informative to consider the limit of small variability in prey. In this case, the spatial variation in growth rate is relatively small compared to the diffusion time across the domain, and we find that

$$\psi = 1 + \psi'(x)$$

with $|\psi'| \ll 1$ and

$$\frac{\partial}{\partial x}\kappa_1\frac{\partial}{\partial x}\psi' \simeq \frac{\sigma - g'(x)}{\kappa_2(x)}.$$

Integrating this last equation from 0 to L gives an estimate of the growth rate enhancement

$$\sigma \simeq \left[\int_0^L \frac{g'(x)}{\kappa_2(x)}\,dx\right]\left[\int_0^L \frac{1}{\kappa_2(x)}\,dx\right]^{-1}. \tag{4.4}$$

When furthermore the variability in the diffusion rate (the swimming term) is also small, so that $|\kappa'| \ll |K_0|$, Eq. (4.4) linearizes even further

$$\sigma \simeq -\frac{1}{K_0 L}\int_0^L g'(x)\,\kappa'(x)\,dx. \tag{4.5}$$

Since the growth rate and swimming rate variations are presumed to be negatively correlated, we therefore find enhancement associated with the patchiness (i.e., the product of g' and κ' is negative so that the right-hand side of (4.5) is positive).

c. Unsteady case. When the prey distribution changes in space and time, we can look at the spatial average of Eq. (4.1) and the equation for the spatial variability. This again can yield useful information in the small amplitude limit. If we use $\overline{(\ )}$ to indicate averaged quantities and $(\ )'$ to indicate deviations from the average, we have

$$\frac{\partial}{\partial t}\bar{b} = \overline{g'(x,t)\,b'(x,t)} \tag{4.6}$$

$$\begin{aligned}\frac{\partial}{\partial t}b'(x,t) = {} & g'(x,t)\bar{b} + [g'(x,t)\,b'(x,t) - \overline{g'(x,t)\,b'(x,t)}] \\ & + \bar{b}\bar{\kappa}_1\frac{\partial^2}{\partial x^2}\kappa'(x,t) + K_0\bar{\kappa}_1\frac{\partial^2}{\partial x^2}b'(x,t) + \left[\frac{\partial}{\partial x}\kappa_1'\frac{\partial}{\partial x}(K_0 b' + \kappa'\bar{b} + \kappa' b')\right. \\ & \left. + \bar{\kappa}_1\frac{\partial^2}{\partial x^2}\kappa' b'\right].\end{aligned} \tag{4.7}$$

Of course, we cannot directly compute the right-hand side of (4.7); however, if we approximate by dropping terms which are quadratic in spatially variable functions (called the "mean field approximation," cf. Herring, 1963), we obtain

$$\frac{\partial}{\partial t}b'(x,t) - K_0\bar{\kappa}_1\frac{\partial^2}{\partial x^2}b'(x,t) \simeq \left[g'(x,t) + \bar{\kappa}_1\frac{\partial^2}{\partial x^2}\kappa'(x,t)\right]\bar{b} \tag{4.8}$$

which shows that $b'(x,t)$ is a linear function of $\bar{b}$; this implies that the mean equation (4.6) will indeed have exponentially growing behavior (except for the time variability in various coefficients). Note that the term κ_1' does not enter, implying that the variation in this part of the diffusion will be relatively ineffectual compared to variations in g and κ_2. The simplest case occurs when the average diffusion rates are time-independent (so that we can set $\kappa_1 = 1$) and when there is a single wavenumber and frequency for the variable growth and diffusion rates

$$\begin{aligned} g'(x,t) &= -a\cos(kx - \omega t) \\ \kappa'(x,t) &= K_2\cos(kx - \omega t)\end{aligned} \tag{4.9}$$

(phase shifts could be considered also). Note that the Eq. (4.8) determining b' is linear, so that we can superimpose many different Fourier components with different frequencies and wavenumbers. Thus a standing wave pattern could be constructed using a leftward and a rightward travelling wave. For the single component (4.9), we solve equation (4.8) [assuming that the changes in $\bar{b}$ occur much more slowly than the

variations in $g'(x, t)$ and $\kappa'(x, t)$] and find the perturbation predator biomass

$$b'(x, t) = -\frac{(a + K_2k^2)K_0k^2}{\omega^2 + K_0^2k^4}\left[\cos(kx - \omega t) - \frac{\omega}{K_0k^2}\sin(kx - \omega t)\right].$$

When we substitute this into (4.6), we find

$$\frac{\partial}{\partial t}\bar{b} = \sigma\bar{b}$$

with the enhancement to the growth rate being

$$\sigma = \frac{a(a + K_2k^2)K_0k^2}{2(\omega^2 + K_0^2k^4)}. \tag{4.10}$$

In the limit of steady prey distribution ($\omega = 0$), this simplifies to

$$\sigma = \frac{a(a + K_2k^2)}{2K_0k^2} \tag{4.11}$$

which reproduces the previous result (4.5, with the substitution of a cosine profile) when a is small compared to K_2k^2.

In general (from 4.10), we find enhancement to the predator growth as the variability in swimming increases, or as the frequency of prey variations decreases. The swimming variability simply enhances the organisms' ability to remain in the regions of high prey and to migrate out of the regions with low prey. The dependence of the growth enhancement on the mean diffusion coefficient, K_0, is more complicated: if the prey pattern is steady, enhancement is increased as the average diffusion goes down. This enhanced growth occurs because some organisms are sitting in high prey patches and their rapid doubling more than compensates for those in low prey environments (Fig. 9). The slower background diffusion permits them to stay longer in the favorable environments. However, if the prey are also varying in time, weak background diffusion decreases the effects of patchiness, since the predators can no longer move into the favorable regions rapidly enough compared to the period of the patch.

d. Numerical solution. For the steady case, we have solved the eigenvalue problem (4.3) numerically and found the enhancement to the growth rate as contoured in Figure 10. The special case (4.9) (with anticorrelation between the swimming speed and the growth rate) has been used. Note that the net growth rate enhancement follows the pattern predicted by (4.11): it is increased by either increasing the variability in the swimming speed (increased K_2) or by making the average diffusion weaker.

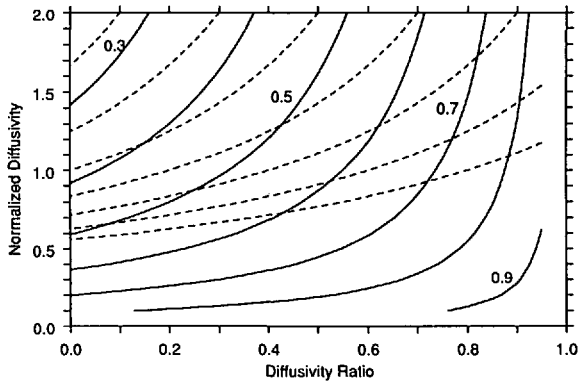

Figure 10. Enhancement of growth rate in predator biomass (σ/a) as a function of the swimming variability—the diffusivity ratio (K_2/K_0)—and the background normalized diffusivity (K_0k^2/a). The solid contours are from the solution of (4.3) plus (4.9), while the dashed contours show the growth rates from the linearized estimate (4.11).

e. Spatial scale and patch structure. If we have more complicated spatial and temporal structure to the prey patch, we must superimpose waves of different k and ω in (4.9). The enhancement from each component is given by (4.10); to get the total, we simply sum over the components of the patch wavenumber-frequency spectrum. If we assume that K_2 is proportional to a, $K_2 = k_2 a$ and that a itself is a linear function of prey concentration at the specified wavenumber and frequency $a = \alpha\hat{C}(k, \omega)$, we have

$$\sigma = \alpha^2 \int dk \int d\omega \frac{(1 + k_2k^2)K_0k^2}{2(\omega^2 + K_0^2k^4)} |\hat{C}|^2. \tag{4.12}$$

This shows that weighting for the high frequency parts of the spectrum is relatively small, the small scale (large k) variability contributes uniformly (i.e., only the net variance is important), and the low frequency, large scale components give the strongest enhancement. Figure 11 shows the weighting factor for different prey space and time scales. The estimate (4.5) for steady state situations is also consistent with the enhancement depending on the *variance* in the prey field:

$$\sigma \simeq \frac{\alpha^2 k_2}{K_0} \frac{1}{L} \int_0^L |C'|^2.$$

Eq. (4.12) permits us to assess the limits of validity of this approximation. In particular, it applies when most of the energy in the prey spectrum falls in the part of the (ω, k) plane where the weighting is constant (see Fig. 11). This corresponds to $\omega \ll K_0k^2$ (prey time scales long compared to diffusion time) and $K_2k^2 \gg a$ (variability of diffusion times small compared to variability in growth rates). Note that these remarks do not mean that this parameter region contributes most strongly

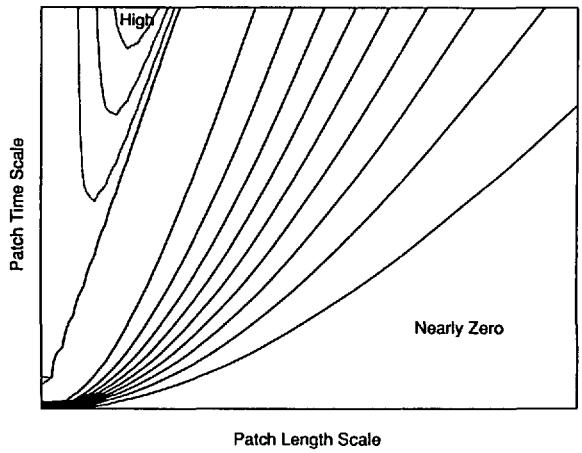

Figure 11. Influence of various spatial and temporal scales of the prey patches on growth enhancement. As an example, for a 1 cm fish larva (as in Fig. 7), the patch wavelengths run from 0 to 100 m and the periods from 0 to 10 days. Light contours indicate the zone which most affects the net growth. In this case, the values are only slightly elevated in this region.

to growth—indeed, the most important part is the low frequency large scale region where the second inequality does not hold—but only marks the region where the enhancement is sensitive only to the net variance, not to the spatial structure.

The formula (4.10) also reveals how the growth rate of different types of organisms would be altered by patchiness in their food source. The ratio σ/a depends on the parameters K_0k^2/a, K_2/K_0, and ω/a. Different organisms might have rather similar ratios K_2/K_0 since these both depend on swimming speeds. The other parameters measure the ratio of the rate for diffusing across a patch compared to the difference in growth rate from inside to outside the patch, K_0k^2/a, and the ratio of patch frequency to growth rate difference. For example, a 1 cm larval fish in 10 m domain diffusing at 100 cm^2/s and a 1 mm copepod in a 1 m domain diffusing at 1 cm^2/s take a similar time (10^4 s) to diffuse across the domain; if their growth rates are similar, we would then find similar enhancement.

5. Effect of turbulent encounter

From the above analysis we have found that microscale patchiness of prey, in the absence of physical diffusion, can significantly enhance predator growth rate. We now examine the combined effects of patch dissipation and increased encounter velocities due to physical diffusion together with variable growth and swimming.

a. Incorporation of turbulence. Physical turbulence is included in the growth and diffusion terms of the predator Eq. (3.11) as follows:

First, turbulent encounter rate is given by the expression of Rothschild and

Osborn (1988) as modified by Evans (1989):

$$E_0 = \sqrt{u^2 + v^2 + 2w^2}\, P(x, t)$$

where E_0 is encounter rate (/s), u and v are prey and predator swimming velocities (cm/s), w is encounter velocity due to physical turbulence (cm/s), and P is prey concentration (# prey/cm). In order to allow for dissipation of prey as well as predators, prey abundance will be computed from an equation analogous to (3.11):

$$\frac{\partial}{\partial t} P = \frac{\partial^2}{\partial x^2} [K_p + K_{ps}(x)] P$$

where K_p is eddy diffusivity and $K_{ps}(x)$ allows for reaggregation of prey thus serving as a generic forcing mechanism for prey patchiness. The distribution of K_{ps} was derived by transforming spatial variance spectra into physical space. In the example below only a simple cosine distribution of K_{ps} is used.

We have not included any feedback from the predator upon the prey field, as appropriate for larval fish which are often too dilute to affect the prey abundance (c.f. Davis, 1984b; Bollens, 1988; Cushing, 1983). We anticipate that the amplitude of prey patches will be lower when the predator can efficiently graze down prey patches, as may occur for the case of copepods.

Second, predator growth rate, g, was linearly related to encounter rate by

$$g = g_1 E_0 + g_2$$

where g_1 (/prey) and g_2 (/s) are constants.

Third, diffusivity, κ, is represented as the sum of physical, K_p, and swimming, K_s diffusivities. Predator swimming diffusivity was inversely related to encounter rate by

$$K_s = k_1 / E_0$$

where k_1 (cm^2/s^2) is a constant.

Substituting these expressions into the predator equation (3.11) gives

$$\frac{\partial}{\partial t} B = (g_1 E_0 + g_2) B + \frac{\partial^2}{\partial x^2} \left[K_p + \frac{k_1}{E_0} \right] B.$$

Physical diffusivity, K_p (cm^2/s) and w were related to surface wind speed, U_{10} (m/s), through the turbulent kinetic energy dissipation rate, ϵ (watts/m^3)

$$K_p = 6.25 \times 10^3 \epsilon$$

and

$$w = 1.9(\epsilon r)^{1/3}$$

(where r (cm) is the eddy separation distance, Rothschild and Osborn, 1988; relation

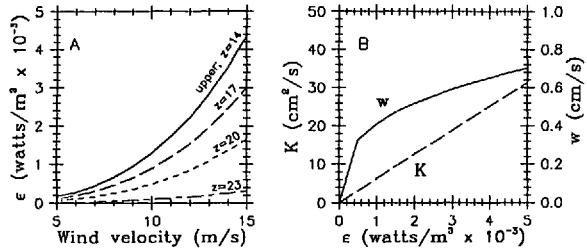

Figure 12. Relationship of physical forcing parameters used to assess the impact of turbulence on patchiness and growth rate. A) Turbulent kinetic energy dissipation rate, ϵ, versus surface wind velocity, U_{10}, for upper (top curve) and lower (all curves) 10 m of the surface mixed layer (from empirical equations in Oakey and Elliot, 1982). Curves for the lower 10 m are for different mixed layer depths, Z_{ml}; ϵ is the same in both upper and lower regions when the mixed layer depth is less than 14 m. B) Physical diffusivity, K_p, and turbulent encounter velocity, w, versus dissipation rate based on equations given in text. The values for dissipation rates are typical for the surface mixed layer in the open ocean.

of K to ϵ taken from Denman and Gargett, 1983, using values for buoyancy and ϵ from Oakey and Elliott, 1982).

Relation of ϵ to U_{10} was taken from Oakey and Elliott (1982) for the upper and lower 10 m of the surface mixed layer

$$\epsilon_{\text{upper}} = 1.33 \times 10^{-6} U_{10}^3$$

and

$$\epsilon_{\text{lower}} = (3.15 \times 10^{-6} - 1.33 \times 10^{-7} Z_{ml}) U_{10}^3.$$

Dissipation increases as a cubic function of wind speed and in the lower layer decreases linearly with mixed layer depth, Z_{ml} (m) (Fig. 12a). Eddy diffusivity is linearly related to dissipation rate, while physically induced encounter velocity increases only as the cube root of ϵ (Fig. 12b). Thus, in this model formulation, K_p scales as the cube of wind velocity while w scales linearly, and, for the lower mixed layer, w decreases as the cube root of mixed layer depth while K_p decreases linearly (Fig. 13).

b. Effects of turbulence on growth. Given these relationships for physically dependent growth and diffusion we can explore the effects of wind mixing and prey patchiness on predator growth rate. We first consider the case of a steady wind at various velocities and examine predator growth with and without prey patchiness and with and without turbulent encounter. We do this for fixed and diffusing prey patches. Finally, we examine the case of variable winds, i.e. time-dependent patchiness. The model was dimensionalized as above (Section 3) for a 1.0 cm haddock larva in a 10 m domain. A simple cosine distribution of K_{ps} gave prey levels proportional to

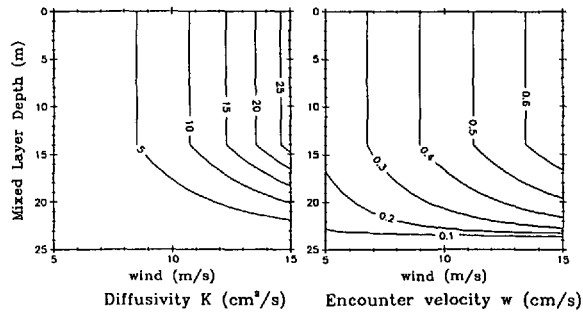

Figure 13. Contours of physical diffusivity, K_p, and encounter velocity, w, in the bottom 10 m of the mixed layer as functions of surface wind speed, U_{10}, and mixed layer depth, Z_{ml}, taken from relationships shown in Figure 12. When mixed layer depth is less than about 15 m, values of K and w are the same as in the upper 5 m. Upper 5 m values are unaffected by mixed layer depth. Note that encounter velocity decreases more rapidly with Z_{ml} and increases more slowly with wind speed than does diffusivity.

1/[cosine + const.] with mean of 15/liter and range 7–30/liter. Growth parameters g_1 and g_2 were chosen such that growth rate ranges from 0.0–0.15 (/d) with a mean of 0.05. We let r = 10 cm to approximate the separation distance of eddies at these scales. Since swimming diffusivity, K_s, is equal to k_1/E_0 and also $K_s = 0.5\ vl$, to find k_1 we let $u = w = 0$ so that $E_0 = vP$ and $l = 1/P$, thus $k_1 = 0.5\ v^2 l/P$. Again we let $l/P = 0.1$ so that the mean free path for predator swimming is 10% of the distance between prey or in this case 3–14 cm. Population growth rate calculated from the model is expressed as ln (B_1/B_0) where B_0 and B_1 are spatially averaged predator biomass at t = 0.0 and 1.0 d, respectively. This growth rate is equivalent to the exponential rate of increase in B over 1 day.

With these parameter values, a steady prey distribution, and physically diffusing predators, we find that, with homogeneous prey, increasing turbulence increases the growth rate from 0.05 to 0.069 (/d) (Fig. 14a) (long dash). In this nonpatchy case the growth enhancement is in general agreement with Rothschild and Osborn (1988). With a prey patch present but without turbulent encounter (i.e., w = 0), growth rate decreases from 0.74 to 0.54 due to physical diffusion of predators (Fig. 14a short dash); higher growth occurs at low turbulence due to predators diffusing into the patch by swimming. With both patchiness and turbulent encounter invoked (Fig. 14a chain dash), growth rate remains relatively high at all wind speeds with a slight minimum (.068/d) at U_{10} = 10 m/s wind.

In this example with a fixed prey patch, we see that, at low turbulence levels, increased growth rate is due largely to predator swimming while at high turbulence levels growth enhancement is due primarily to higher physically induced encounter velocities (Fig. 14). A minimum in growth occurs because, at wind speeds $<$10 m/s, patch dissipation rate increases more rapidly with wind speed than does turbulent

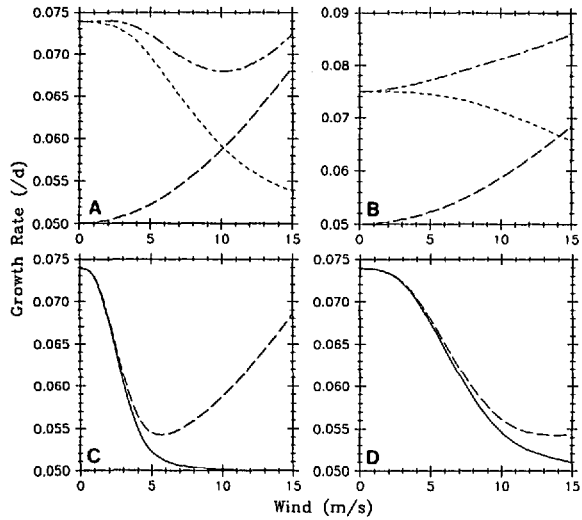

Figure 14. Differential effects of patchiness, turbulent encounter velocity, and turbulent diffusion on predator growth rate. Weight specific growth rate of predator biomass is plotted versus wind speed (m/s, ≈ knots/2) for stationary (A-B) and passively diffusing (C-D) prey patches in upper (A-C) and lower (D) parts of the surface mixed layer. Predators diffuse in all cases due to physical turbulence and swimming. Curves in (A-B) represent growth rate of predator in: homogeneous prey with turbulent encounter (long dash); patchy prey without turbulent encounter (short dash); and patchy prey with turbulent encounter (chain dash). Curves in (C-D) are for passively diffusing prey patch with (dash) and without (solid) turbulent encounter. Model was parameterized for a 1 cm haddock larvae swimming in a patch of copepod nauplii. Prey patch size was 10 m in (A, C, and D) and 3 m in (B).

encounter velocity, whereas, at higher wind speeds, the rate of turbulent encounter becomes the dominant factor controlling growth rate.

The chosen parameter values cause predator swimming diffusion to be somewhat lower (2-9 cm^2/s) than turbulent diffusion (K_p = 1-38 cm^2/s, upper mixed layer). If we assume a patch size of 3 m rather than 10 m (keeping the range in prey concentration the same), the relative rate of swimming diffusion increases by a factor of 10 and turbulence then causes an overall increase in growth rate (Fig. 14b); note that patchiness with turbulence yields much higher growth than found with turbulence and homogeneous prey. Thus swimming diffusion has a greater impact on growth rate as patch size decreases. This is because physical diffusivity scales roughly with distance (actually with the 4/3 power of length) but predator swimming speed is unaffected by reduction in domain size from 10 to 3 m.

If we now let an initial prey patch (10 m) diffuse passively due to turbulent mixing without any reaggregation (i.e., letting K_{ps} = 0 after initial prey patch is formed), we find that, in the upper layer, the growth rate falls off sharply at low wind speeds due to dissipation of prey (Fig. 14c), but increases again at higher wind speeds in the case

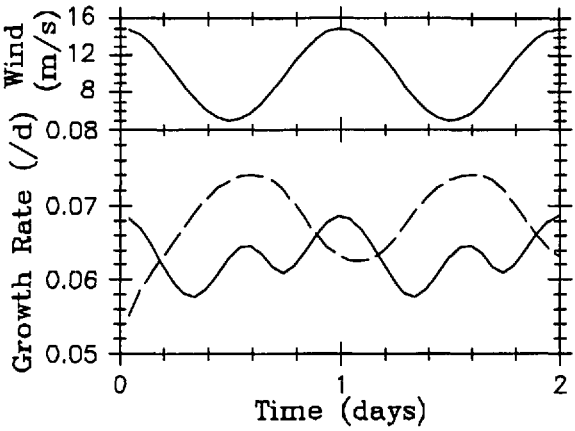

Figure 15. Effects of temporally varying winds (top panel) on growth of plankton in upper (solid) and lower (dashed) 10 m of the surface mixed layer. In upper layer, growth is enhanced during low and high winds due to increased patchiness and turbulent encounter, respectively. Intermediate winds destroy patchiness but do not increase turbulent encounter enough to compensate. In the lower mixed layer, turbulence in weaker, and, although high winds diffuse the patchiness, turbulent encounter velocities remain small.

including enhancement of encounter due to turbulence. In the lower layer (Fig. 14d), (Z_{ml} = 23 m), the decrease in growth rate is similar to the fixed patch case (Fig. 14a short dash) but growth at higher wind speeds is lower because the turbulence is too mild to substantially increase encounter rate (Fig. 14d). Decreasing the domain size (or increasing predator swimming diffusion) was found to have little effect on growth rate in the latter case since prey patch dissipation is the dominant cause of growth rate reduction.

The time-dependent solution with varying winds (Fig. 15) reflects the results of the steady wind case. With wind velocity varying daily from 5–10 m/s, growth in the upper mixed layer (solid line) is greatest at minimal and maximal winds and lowest at intermediate wind speeds. As in the steady case, low winds allow predator/prey patch formation while high winds cause significant turbulent encounter. Intermediate winds destroy patchiness but are not strong enough to substantially increase turbulent encounter velocity. In the lower mixed layer (Z_{ml} = 23 m, dashed line), increasing winds cause patch dissipation but the turbulence at high wind velocities remains too low to significantly increase encounter velocity. In this time-dependent case we invoked reaggregation of prey ($K_{ps} > 0$) at a rate sufficient to overcome physical diffusion at the lowest wind speeds. As discussed below, however, this recovery rate requires unrealistically large swimming speeds on the part of the prey, and it is unlikely that prey swimming can cause micropatchiness in the ocean (see Discussion).

6. Relation of growth rate to mortality rate and recruitment

The above analysis suggests strongly that micropatchiness and turbulence can cause variations in planktonic growth rates. Although relative deviations as high as 50% were found, in some cases the changes may be relatively small ($< 10\%$). We now examine the relationship between growth and mortality rates and their relative importance in the recruitment process. Our goal is to determine how deviations in mean pre-recruit growth rate translate into recruitment deviations. First order estimates of this kind, for larval fish (Houde, 1982), show that relatively minor changes in development time can lead to large variations in recruitment. We present a second order analysis including weight and time dependent parameters. Recruitment is considered as the number of individuals reaching a particular body size (weight) per unit time, rather than age class. This is a useful definition, since, for most planktonic organisms, age is difficult, if not impossible, to determine. This analysis can also be applied to age based recruitment as discussed below.

The change in numbers of individuals within a cohort over time can be expressed

$$\frac{\partial}{\partial t} N + \frac{\partial}{\partial w} gN = -mN$$

where $N(w, t)$ is the number per unit weight class at time t, $g(w)$ and $m(w)$ are weight dependent growth and death rates, and w is individual body weight. The middle term represents individuals passing into and out of a given size range due to growth.

We express weight dependent growth as

$$\frac{dw}{dt} = g = Gq(w)$$

where $q(w)$ is a weight-dependent growth function (time invariant), and G is the instantaneous growth coefficient which varies between generations but is constant within a generation.

Integration over the pre-recruit period gives

$$\int_{w_0}^{w_r} \frac{dw}{q(w)} = Gt_r$$

where w_0 and w_r are initial and recruited body weights, respectively, and t_r is the duration of the pre-recruit stage or the time to reach w_r. t_r varies between generations due to variations in G.

In the simplest case, for a cohort of uniform weight spawned at a single time, $t = 0$, we have

$$\frac{dN}{dt} = -m(w(t))N$$

Intergration over the pre-recruit phase gives

$$\ln \frac{R}{N_0} = -\int_0^{t_r} dt\, m(w(t))$$

where N_0 and R are initial and recruited number in the cohort, respectively.

With respect to weight we have

$$\ln \frac{R}{N_0} = -\frac{1}{G}\int_{w_o}^{w_r} dw\, \frac{m}{q}$$

and relating any two generations, 1 and 2, gives

$$\frac{R_2}{N_{0_2}} = \left(\frac{R_1}{N_{0_1}}\right)^{G_1/G_2}.$$

It can be shown that this equation also holds for cohorts spawned over a period of time and for cohorts having a nonuniform initial weight distribution if this distribution is narrow. From this equation, one can calculate the range in growth rates which would be required to account for observed variations in recruitment if these variations were due solely to changes in growth rate. In general, small changes in growth rate between generations can cause large changes in recruitment. As an example, we can determine the potential impact of planktonic larval growth on recruitment to a fixed age class, as for fish populations. In this case, the above analyses apply to the planktonic phase of life, and, to examine the contribution of larval growth by itself, we assume post-planktonic, pre-recruit mortality rate to be zero. We have calculated R/N_0 for Georges Bank haddock from VPA (virtual population analysis) estimates of stock size between 1963 and 1983 (Table 1). Selecting R_1/N_{0_1} equal to the 1974 value of 1.92×10^{-6} (closest to the mean, 1.7×10^{-6}), the ratios of growth (Table 1) were calculated from

$$\frac{G_1}{G_2} = \frac{\ln \dfrac{R_2}{N_{0_2}}}{\ln \dfrac{R_1}{N_{0_1}}}.$$

As can be seen from Table 1, most of the recruitment variability can be accounted for by relatively small deviations in growth (coefficient of variation = 14%). These results also apply when post-planktonic mortality rate is nonzero, but small, relative to larval mortality rate, as is usually the case. It is obvious from these calculations that variable growth is potentially a very important component of recruitment variability. Although larval mortality may not correlate well with number of first year recruits due to interannual variation in juvenile mortality (Peterman *et al.,* 1988), as discussed below, this does not mean the larval stage is unimportant to recruitment.

Table 1. Recruitment/eggs and ratio of pre-recruit growth in 1974, G_1, to that in each other year, G_2, from 1963–1983, assuming recruitment variability is due solely to changes in growth rate according to equation given in text.

Year	R/E	G_1/G_2
1963	8.960×10^{-6}	0.883
1964	0.710×10^{-6}	1.076
1965	0.074×10^{-6}	1.247
1966	0.172×10^{-6}	1.183
1967	0.009×10^{-6}	1.410
1968	0.035×10^{-6}	1.300
1969	0.296×10^{-6}	1.140
1970	0.020×10^{-6}	1.350
1971	1.250×10^{-6}	1.033
1972	3.760×10^{-6}	0.949
1973	4.070×10^{-6}	0.943
1974	1.920×10^{-6}	1.000
1975	24.61×10^{-6}	0.806
1976	3.150×10^{-6}	0.962
1977	0.330×10^{-6}	1.134
1978	5.700×10^{-6}	0.917
1979	0.500×10^{-6}	1.100
1980	0.330×10^{-6}	1.134
1981	0.144×10^{-6}	1.197
1982	0.212×10^{-6}	1.167
1983	0.300×10^{-6}	1.141
		mean ± S.D. = 1.085 ± 0.27

On the contrary, for a given level of juvenile mortality, fluctuations in larval growth or mortality rate will translate into recruitment variation.

7. Discussion

The above results suggest strongly that microscale patchiness in planktonic prey concentration can enhance predator growth and recruitment success. As modeled here, physical turbulence, at intermediate levels, causes patch dissipation and reduced growth, whereas, at higher levels, it causes growth to be restored to original, low-turbulence, values due to increasing encounter velocities. Variations in population growth rate due to turbulence and micropatchiness, even if small ($< 10\%$), can cause large fluctuations in recruitment by affecting duration of the pre-recruit life stage. Such growth rate variations have the same impact on recruitment as equivalent deviations in mortality rate.

We have shown that biological diffusion induced by nondirected swimming can cause rapid aggregation of predators into micropatches of prey. With homogeneous prey, this mechanism causes dispersion of predators. In the absence of swimming,

predators will grow faster at patch center and build up biomass more rapidly in this region, but this rate of accumulation is slow and insignificant compared with aggregation due to swimming diffusion. This model of swimming diffusion is conservative since we assume nondirectional swimming on the part of the organism. In a detailed model of larval anchovy, Vlymen (1977) found that, with directed swimming, larvae could greatly enhance their growth rates by feeding in micropatches of prey. An assumption of Vlymen's model was that the highest probable direction for swimming was toward the center of a patch. It is unlikely, however, that a larva can detect, a priori, the center of a patch several body lengths away, so that this form of directed swimming does not appear plausible. As Vlymen (1977) points out, though, it is unlikely that forward and reverse directions have equal probability, the larva being more efficient at moving forward or turning up to 90°. Any sort of directed motion would cause the growth enhancement induced by micropatchiness to be even more pronounced than our models predict since the animals would reach patch center more rapidly and would counteract the dissipative effects of turbulence more effectively than in the purely random case.

The mechanism of biological "antidiffusion" or random walk up a resource gradient has been discussed by other investigators (e.g., Fenchel and Finlay, 1984, for protozoans in a vertical gradient of nutrients) and the form of the diffusion term in Eq. (3.1) is discussed in Okubo (1980). By coupling this diffusion term with the growth term and parameterizing the model for larval fish as well as examining the nondimensional case, we have found that microscale patchiness of prey over a range of <1 to 10 m can substantially increase growth rate for zooplankton ranging in size from copepods to fish larvae, even when the conservative assumption of nondirected swimming is applied. These results should be independent of feeding mode (e.g., suspension vs. raptorial) if the mean free path of swimming is negatively related to food concentration.

Although turbulence increases encounter velocity between predator and prey, low to intermediate levels of turbulence cause decreases in encounter rate, and thus growth rate, by dissipation of predator-prey patches. High levels of turbulence, however, yield encounter velocities which are large enough to compensate for the reduction in prey density due to homogenization. The model of Wroblewski (1984) for northern anchovy showed that turbulence dissipated patches of dinoflagellate prey causing reduced ingestion. He also found that vertical swimming by the algae was more important than algal growth in maintaining a vertical layer of prey against turbulent mixing. His model did not include larval swimming or the effects of turbulence on encounter velocity. Peterman and Bradford (1987) found an inverse relation between wind speed and larval anchovy survival, and suggested micropatch formation during calm periods increased survival. Alcaraz *et al.* (1985) found that turbulence altered the evolution of phytoplankton biomass in laboratory microcosm experiments and suggested that increased zooplankton grazing might have been responsible. Observations of feeding in tethered copepods suggest that turbulence

increases ingestion rate (unless food is already saturating), although it also may cause behavioral modifications which reduce feeding rate (Marasse *et al.*, 1990; Costello *et al.*, 1990).

The rate of turbulent diffusion of a prey patch can be reduced, compared to the purely passive case, by invoking a reaggregation mechanism which can be viewed as a generic source for the patchiness. The minimum in predator growth rate (Fig. 14C) is higher when prey swimming diffusion, K_{ps}, is nonzero. Prey swimming rates required to counteract turbulent dissipation are unrealistically high, however, and it is unlikely that prey, such as copepod nauplii, would be able to form micropatches in the ocean on scales of 10 m by random swimming. The mean free path and swimming speed of a nauplius is likely much less than 1 cm and 1 cm/s, respectively, giving diffusion rate of $\ll 1$ cm^2/s which is low relative to the physical diffusivity (1-28 cm^2/s). Since prey doubling time is even slower, it is an engima as to how prey micropatches are formed in the ocean. It is possible that micropatches of egg-laying adult copepods could produce micropatches of nauplii, but given swimming speeds of adult copepods it is unlikely that they would be able to overcome the physical turbulence at the 10 m scale either. Micropatches of much smaller organisms such as protozoans have also been found (Owen, 1989) and swimming abilities of these organisms (although impressive on a body length/s basis) or their growth rates are clearly insufficient to form 10 m micropatches.

It is likely therefore that formation of prey micropatches in the ocean is driven by eddy diffusion acting on larger scale biological gradients such as those in frontal regions. Although diffusion in the present model is of the simple Fickian type, the actual mixing process is due to advection by eddies at decreasing scales. Large patches are stretched and broken into smaller ones as mixing progresses. Divergent flow from a frontal region having a biological gradient could eventually lead to microscale patchiness. Owen (1989) found that wind mixing reduces patch size and amplitude agreeing with models of tracer dispersal (Holloway and Kristmannsson, 1984). In the present model, mixing does not affect the scale of patchiness but rather represents a reduction of the ensemble average of patch amplitude. Our representation of diffusion is likely to cause a more rapid decrease in growth rate than actually would result from prey dissipation. If the initial prey patch forms into smaller and smaller patches, predators would reach the center of these smaller patches more rapidly than they would a single larger patch of the same amplitude.

The significant effect of growth rate on recruitment has been discussed by Houde (1982) for larval fish. Our analysis reveals that changes in growth rate are as important as changes in mortality rate in determining recruitment. Although starvation mortality may not be as important as once thought (Hjort, 1914; Lasker, 1975; Laurence, 1985a), this does not mean that food is nonlimiting to survival. If food levels are below saturation for feeding and growth, deviations in food supply between cohorts will be as significant to recruitment success as similar deviations in mortality. Finally, the recent findings of Peterman *et al.* (1988) that recruitment in larval

anchovy is uncorrelated with larval survival should not be taken to mean that larval survivorship does not contribute to recruitment. Indeed for any given cohort, the planktonic phase, although short, accounts for at least one third of the total pre-recruit mortality. Unless there are strong compensatory mechanisms operating during the juvenile phase, larval survivorship will have a large impact on recruitment. Even without density dependence, however, this impact may not be correlated with interannual variation in recruitment, since deviations in post-planktonic survival can be large, thus obscuring contributions of the larval stage.

8. Conclusions

Using a series of simple diagnostic models we have found that, under limiting food conditions:

(1) Individual growth of a predator (or herbivore) is approximately exponential and linearly related to food concentration over time scales relevant to micropatchiness (> 1 h).

(2) Random swimming by consumers, when handling time and/or swimming speed are negatively correlated with food concentration, leads to net migration into areas of high prey.

(3) Aggregation into high food areas causes a significant increase in predator population growth for both static and transient prey patches.

(4) Physical turbulence, at intermediate levels (upper mixed layer with winds at 5 m/s), will reduce this growth rate by homogenizing predator/prey patches, but at higher levels (winds at > 10 m/s) will restore growth to the low turbulence values due to more frequent encounters between predator and prey.

(5) Changes in growth rate, even if slight, cause large deviations in recruitment; growth rate variations are as important to recruitment success as are equivalent changes in mortality rate.

Acknowledgments. This work was supported by NSF grant OCE-8700562 and ONR grant N00014-89-J-1358. We are indebted to E.B. Cohen (NMFS, Woods Hole) for generously providing egg/recruit data for Table 1. We also thank K. L. Denman and an anonymous reviewer for their critical comments on the manuscript. Contribution number 7613 of the Woods Hole Oceanographic Institution.

APPENDIX

Solutions to linearized growth model

We begin linearizing the growth model (2.9-10) by expanding the logarithm in the ingestion curve:

$$\ln (a_+ - G/w/w_0)^m) = \ln (a_+) + \ln \left(1 - \frac{Gw_0^m}{a_+ w^m}\right)$$

$$\simeq \ln (a_+) - \frac{Gw_0^m}{a_+ w^m}$$

which is valid if the gut is never full. Eq. (2.10) then becomes

$$\frac{DG}{Dt} = I_0\left(\frac{w}{w_0}\right)^m\left(\frac{C}{C_0}\right) - I_0\left(\frac{C}{C_0}\right)G\frac{1}{a_+\ln(a_+/a_-)} - a_gG. \tag{A.1}$$

When the powers m and n are chosen to be one, the growth equations become simply

$$\frac{Dw}{Dt} = a_e a_g G - \hat{a}_r w \tag{A.2}$$

$$\frac{DG}{Dt} = \hat{I}Cw - (\hat{I}_g C + a_g)G \tag{A.3}$$

and

$$\hat{a}_r = a_r/w_0, \qquad \hat{I} = I_0/Cw_0, \qquad \hat{I}_g = I_0/C_0 a_+ \ln(a_+/a_-).$$

Eqs. (A.2–3) have exponential solutions with growth rates

$$\sigma = -\tfrac{1}{2}(\hat{a}_r + a_g + \hat{I}_g C) \pm [(a_g + \hat{I}_g C - \hat{a}_r)^2 + 4a_e a_g \hat{I}C]^{1/2}. \tag{A.4}$$

The plus sign corresponds to the growing root if one exists. In the food-limited range, the root corresponding to the growing solution has an e-folding rate

$$\sigma \simeq -\hat{a}_r + \frac{a_e a_g}{(a_g - \hat{a}_r)}\hat{I}C \tag{A.5}$$

(since $a_g > \hat{a}_r$). Thus we demonstrate exponential growth occurs in this case when there is sufficient food and also that the growth rate is a linear function of the food concentration when C is small enough. Note also the necessity for sufficient food in order to have positive growth; this also appears in (A.4) as the requirement that

$$(a_e a_g \hat{I} - \hat{a}_r \hat{I}_g)C > \hat{a}_r a_g$$

for σ to be positive. When a_g is large compared to a_r, we recover the same requirement as that set by (A.5).

Symbols used in the models (listed by Section)

Section 2

t	time
T	mass in body tissue
S	mass in storage
TS	tissue growth (mass/time)
DS	changes in storage (mass/time)
G	gut mass
w	weight of organism
w_0	initial weight

I	ingestion (mass/time)
A	assimilation (mass/time)
Eg	egestion (mass/time)
RE	respiration and excretion (mass/time)
E	encounter rate (number/time)
$\mathscr{F}$	average foraging/filtering rate (volume/time)
F	mass of food arriving per unit time
C	food concentration (mass/volume)
$\overline{M}$	average mass of a prey particle
M_i	mass of i^{th} food particle
$\mathscr{G}$	gaussian
t_i	time of arrival of i^{th} particle
τ	prey handling time
C_0	scale value for concentration (1 μgC/l)
E_0	encounter rate for predators of weight w_0 in food concentration C_0 (number/time)
m	power for dependence of encounter on predator weight
F_i	probability for ingestion of a particle
a_+	maximum gut mass for an organism of weight w_0
s	power for increase in maximum gut mass with organism weight
M	prey mass
$\mathscr{P}$	probability density function for prey mass
I_0	ingestion rate for organisms with $w = w_0$, $G = 0$, $C = C_0$ (mass/time)
$M_{\min}$	lower limit on prey mass
a_-	lower limit for a predator of weight w_0
a_e	fraction of food lost from gut by assimilation
a_g	rate of gut evacuation (1/time)
a_r	respiration/excretion rate for a predator of weight w_0 (mass/time)
n	power dependence of RE on weight
$\hat{G}$	$G/(w/w_0)^m$
B	biomass
g	exponential growth coefficient (1/time)
Section 3	
x	spatial coordinate
κ_1	"standard" part of diffusivity
κ_2	"biological" part of diffusivity
κ	"biological" diffusivity in case κ_1 = const. (distance^2/time)

K_0	mean "biological" diffusivity (distance^2/time)
K_2	amplitude of variable "biological" diffusivity (distance^2/time)
b_l	left-moving biomass
b_r	right-moving biomass
b_0	stopped biomass
v	swimming speed (distance/time)
T	rate of turning (1/time)
S	rate of stopping (1/time)
R	rate of starting (1/time)
k	wavenumber (1/distance)
w	frequency (1/time)
b	mean part of growth rate g (1/time)
a	variable part of growth rate (1/time)
l	mean free path (distance)
Section 4	
$g_0(t)$	spatial average mean growth rate (1/time)
$g'(x, t)$	spatially variable growth rate (1/time)
$\kappa'(x, t)$	spatially variable "biological" diffusivity (distance^2/time)
K_2	amplitude of variability in κ' (distance^2/time)
σ	population growth rate (1/time)
$b(x, t)$	biomass normalized by that existing in the absence of prey patchiness
$\psi(x)$	eigenfunction $b(x, t)\kappa_2(x) \exp(-\sigma t)$
$\psi'(x)$	spatial variation in the eigenfunction
L	domain scale (periodicity) (distance)
α	proportionality between growth rate and prey concentration (volume/mass/time)
$\hat{C}$	space-time Fourier amplitude of prey concentration (mass distance time/volume)
C'	spatially varying part of prey concentration (mass/volume)
Section 5	
E_0	encounter rate in presence of turbulence (number of prey/time)
u	prey swimming speed (distance/time)
v	predator swimming speed (distance/time)
w	encounter velocity associated with turbulence (distance/time)
$P(x, t)$	prey biomass

K_p	physical eddy diffusivity for prey (distance^2/time)
K_{ps}	reaggregation for prey (distance^2/time)
K_s	swimming diffusivity (distance^2/time)
k_1	proportionality between swimming diffusivity and inverse encounter rate (distance^2/time)
g_1	proportionality between growth rate and encounter rate (1/prey number)
g_2	constant growth rate term (1/time)
ϵ	kinetic energy dissipation rate (power/volume)
ϵ_{upper}	KE dissipation in upper mixed layer
ϵ_{lower}	KE dissipation in lower mixed layer
r	eddy separation distance
U_{10}	wind speed at 10 m
Z_{ml}	depth of mixed layer
Section 6	
N	number in cohort
$m(w)$	mortality rate (1/time)
$g(w)$	growth rate (weight/time)
G	growth coefficient for different cohorts (weight/time)
$q(w)$	weight dependent part of g (nondimensional)
w_0	initial weight
w_r	weight required for recruitment
t_r	time of recruitment
R	recruited number
N_0	initial number

REFERENCES

Alcaraz, M., E. Saizm, C. Marrase and D. Vaque. 1988. Effects of turbulence on the development of phytoplankton biomass and copepod populations in marine microcosms. Mar. Ecol. Prog. Ser., *49,* 117–125.

Bollens, S. M. 1988. A model of predatory impact of larval marine fish on the population dynamics of their zooplankton prey. J. Plankton Res., *10,* 887–906.

Bolz, G. R., and R. G. Lough. 1983. Growth of larval Atlantic cod, *Gadus morhua,* and haddock, *Melanogrammus aeglefinus,* on Georges Bank, spring 1981. Fish Bull., *81,* 827–836.

Costello, J. H., J. R. Strickler, C. Marrase, G. Trager, R. Zeller and A. J. Freise. 1990. Grazing in a turbulent environment: I. Behavioral response of a calanoid copepod, *Centropages hamatus.* Proc. Nat. Acad. Sci., *87,* 1648–1652.

Cushing, D. H. 1983. Are fish larvae too dilute to affect the density of their food organisms? J. Plankton Res., *5,* 847–854.

Davis, C. S. 1984a. Interaction of a copepod population with the mean circulation on Georges Bank. J. Mar. Res., *42,* 573–590.

—— 1984b. Predatory control of copepod seasonal cycles on Georges Bank. Mar. Biol., *82,* 31–40.

Denman, K. L. and A. E. Gargett. 1983. Time and space scales of vertical mixing and advection of phytoplankton in the upper ocean. Limnol. Oceanogr., *28,* 801–815.

Denman, K. L. and A. W. Herman. 1978. Space-time structure of a continental shelf ecosystem measured by a towed porpoising vehicle. J. Mar. Res., *36,* 693–714.

Evans, G. T. 1989. The encounter speed of moving predator and prey. J. Plankton Res., *11,* 415–417.

Fasham, M. J. R. 1978. The statistical and mathematical analysis of plankton patchiness. Oceanogr. Mar. Biol. Ann. Rev., *16,* 43–79.

Fenchel, T. and B. J. Finlay. 1984. Geotaxis in the cilliated protozoan *Loxodes.* J. Exp. Biol., *110,* 17–33.

Gerrittsen, J. and J. R. Strickler. 1977. Encounter probabilities and community structure in zooplankton: a mathematical model. J. Fish. Res. Bd. Can., *34,* 73–82.

GLOBEC, 1988. Global Ocean Ecosystem Dynamics. Report of a workshop on global ocean ecosystem dynamics. Wintergreen, Va. May, 1988. Published by Joint Oceanogr. Inst. Inc., Washington, D.C. 131 pp.

Haury, L. R. and P. H. Wiebe. 1982. Fine-scale multi-species aggregations of oceanic zooplankton. Deep Sea Res., *29,* 915–921.

Herring, J. R. 1963. Investigation of problems in thermal convection. J. Atmos. Sci., *20,* 325–338.

Hjort, J. 1914. Fluctuations in the great fisheries of northern Europe viewed in the light of biological research. Rapp. P.-v. Reun. Cons. Perm. int. Explor. Mer, *20,* 1–228.

Holloway, G. and S. S. Kristmannsson. 1984. Stirring and transport of tracer fields by geostrophic turbulence. J. Fluid Mech., *141,* 27–50.

Houde, E. D. 1982. Micro- and fine-scale biology, *in* Fish Ecology III. A Foundation for REX-Recruitment Experiment. Univ. of Miami, CIMAS. B. J. Rothschild and C. Rooth, eds., pp. 99–125.

Hunter, J. R. and G. L. Thomas. 1974. Effect of prey distribution and density on the searching and feeding behavior of larval anchovy *Engraulis mondax Girard, in* The Early Life History of Fish, J. H. S. Blaxter, ed., Springer-Verlag, NY.

Huntley, M. and C. Boyd. 1984. Food-limited growth of marine zooplankton. Am. Nat., *124,* 455–478.

Ivlev, V. S. 1955. Experimental Ecology of the Feeding of Fishes. Pischepromizdat, Moscow. 302 p. (Transl. from Russian by Scott, D.) New Haven: Yale University Press (1961).

Kiorboe, T., F. Mohlenberg and K. Hamburger. 1985. Bioenergetics of the planktonic copepod *Acartia tonsa*—Relation between feeding, egg-production and respiration, and composition of specific dynamic action. Mar. Ecol. Progr. Ser., *26,* 85–97.

Lampert, W. 1986. Response of the respiratory rate of *Daphnia magna* to changing food conditions. Oecologia, *70,* 495–501.

Landry, M. R., R. P. Hassett, V. Fagerness, J. Downs and C. J. Lorenzen. 1984. Effect of food acclimation on assimilation efficiency of *Calanus pacificus.* Limnol. Oceanogr., *29,* 361–364.

Lasker, R. 1975. Field criteria for survival of anchovy larvae: the relationship between inshore chlorophyll maximum layers and successful first feeding. Fish. Bull. U.S., *73,* 453–462.

Lasker, R. and J. R. Zweifel. 1978. Growth and survival of first-feeding northern anchovy larvae (*Engraulis mordax*) in patches containing different proportions of large and small prey, *In* Spatial pattern in Plankton Communities, J. H. Steele, ed., Plenum Press, NY, 470 pp.

Laurence, G. C. 1985a. A report on the development of stochastic models of food limited growth and survival of cod and haddock larvae on Georges Bank, *in* Growth and survival of

larval fishes in relation to the trophodynamics of Georges Bank cod and haddock, G. C. Laurence and R. G. Lough, eds. NOAA Technical Memorandum, NMFS-F/NEC-36.

—— 1985b. Nutrition and trophodynamics of larval fish. Review concepts, strategic recommendations and options, *in* Growth and Survival of Larval Fishes in Relation to the Trophodynamics of Georges Bank Cod and Haddock, G. C. Laurence and R. G. Lough, eds. NOAA Technical Memorandum, NMFS-F/NEC-36.

Mackas, D. L. and E. P. Anderson. 1986. Small-scale zooplankton community variability in a northern British Columbian fjord system. Estuar. Coast. Shelf Sci., *22,* 115–142.

Marine Zooplankton Colloquium. 1989. Future marine zooplankton research—a perspective. Mar. Ecol. Prog. Ser., *55,* 197–206.

Marrase, C., J. H. Costello, T. Granata and J.R. Strickler. 1990. Grazing in a turbulent environment: II. Energy dissipation, encounter rates, and efficacy of feeding currents in *Centropages hamatus.* Proc. Natl. Acad. Sci., *87,* 1653–1657.

Marshall, S. M. and A. P. Orr. 1955. The Biology of a Marine Copepod, *Calanus finmarchicus* (*Gunnerus*). 180 pp. Edinburgh: Oliver and Boyd.

Miller, C. B. and D. C. Judkins. 1981. Design of pumping systems for sampling zooplankton, with descriptions of two high-capacity samplers for coastal studies. Biol. Oceanogr., *1,* 29–56.

Munk, P. and T. Kiorboe. 1985. Feeding behaviour and swimming activity of larval herring (*Clupea harengus*) in relation to density of copepod nauplii. Mar. Ecol. Prog. Ser., *24,* 15–21.

Newall, G. F. 1963. Distribution for the smallest distance between any pair of *k*th nearest neighbor random points on a line, *in* Proceedings of the Symposium on Time Series Analysis, M. Rosenblatt, ed. John Wiley and Sons, Inc., NY, 497 pp.

Oakey, N. S. and J. A. Elliott. 1982. Dissipation within the surface mixed layer. J. Phys. Oceanogr., *12,* 171–185.

Okubo, A. 1980. Diffusion and ecological problems: mathematical models, *in* Biomathematics, v 10, Springer Verlag, NY.

Owen, R. W. 1981. Microscale patchiness in the larval anchovy environment. Rapp. P.-v. Reun. Cons. Int. Explor. Mer., *178,* 364–368.

—— 1989. Microscale and finescale variations of small plankton in coastal and pelagic environments. J. Mar. Res., *47,* 197–240.

Peterman, R. M and M. J. Bradford. 1987. Wind speed and mortality rate of a marine fish, the northern anchovy, *Engraulis mordax.* Science, *235,* 354–356.

Peterman, R. M., M. J. Bradford, N. C. H. Lo and R. D. Methot. 1988. Contribution of early life stages to interannual variability in recruitment of northern anchovy (Engraulis mordax). Can. J. Fish. Aquat. Sci., *45,* 8–16.

Pieper, R. E. and D. V. Holliday. 1984. Acoustic measurements of zooplankton distributions in the sea. J. Cons. Int. Explor. Mer., *41,* 226–238.

Platt T. and K. Denman. 1978. The structure of pelagic marine ecosystems. Rapp. P.-v. Reun. Cons. int. Explor. Mer, *173,* 60–65.

Reeve, M. R. 1980. Comparative experimental studies on the feeding of chaetognaths and ctenophores. J. Plankton Res., *2,* 381–393.

Roache, P. J. 1982. Computational Fluid Dynamics, Hermosa Publishers, Albuquerque, NM., 446 pp.

Rothschild, B. J. and T. R. Osborn. 1988. Small-scale turbulence and plankton contact rates. J. Plankton Res., *10,* 465–474.

Rothschild, B. J. and C. G. H. Rooth, eds. 1982. Fish Ecology III. A foundation for REX-Recruitment Experiment. Univ. of Miami, CIMAS, 392 pp.

Sameoto, D. D. 1978. Zooplankton sample variation on the Scotian shelf. J. Fish. Res. Bd. Can., *35,* 1207–1222.

Sheldon, R. W., A Prakash and W. H. Sutcliffe. 1972. The size distribution of particles in the ocean. Limnol. Oceanogr., *17,* 327–340.

Stevens, W. L. 1939. Solution to a geometrical problem in probability. Ann. Eugen., *9,* 315–320.

Vidal, J. 1980. Physioecology of zooplankton. IV. Effects of phytoplankton concentration, temperature, and body size on the net production efficiency of *Calanus pacificus.* Mar. Biol., *6,* 203–211.

Vlymen, W. J. 1977. A mathematical model of the relationship between larval anchovy (*Engraulis mordax*) growth, prey microdistribution, and larval behavior. Env. Biol. Fish., *2,* 211–233.

Wroblewski, J. S. 1984. Formulation of growth and mortality of larval northern anchovy in a turbulent feeding environment. Mar. Ecol. Prog. Ser., *20,* 13–22.

Received *10 July, 1990;* revised *31 Janaury, 1991.*